THE ORE MINERALOGY OF THE TV AND JEFF VOLCANOGENIC MASSIVE SULFIDE DEPOSITS IN NORTHWESTERN BRITISH COLUMBIA, CANADA

by

Edgar Cole Eck

A thesis submitted to the Faculty and the Board of Trustees of the Colorado School of Mines in partial fulfillment of the requirements for the degree of Master of Science (Geology).

Golden, Colorado

Date _____

Signed: _____

Edgar Cole Eck

Signed: _____

Dr. Thomas Monecke

Thesis Advisor

Golden, Colorado

Date _____

Signed: _____

Dr. Wendy Bohrson

Professor and Department Head of

Geology and Geological Engineering

ABSTRACT

The precious metal-rich TV and Jeff volcanogenic massive sulfide deposits are located about ~10 km south of the world-class Eskay Creek deposit in the Iskut River area of northwestern British Colombia, Canada. The deposits are hosted by volcanic successions that form part of the Jurassic Hazelton Group. Drill core samples were collected from multiple holes intersecting the precious metal mineralization to identify the ore minerology, with particular emphasis being placed on the study of the mineralogical sequestration of the precious metals. A combination of reflected light microscopy, scanning electron microscopy, automated mineralogy, electron microprobe analysis, and laser ablation-inductively coupled plasma-mass spectroscopy was used to study the ore mineralogy. Paragenetic relationships in the ores show that three distinct stages can be distinguished ranging from pre-ore sulfide formation to metamorphic recrystallization. Pyrite is the most abundant sulfide phase at the TV and Jeff deposit occurring as framboidal pyrite, As-poor and As-rich subhedral to euhedral grains, porphyroblasts, and recrystallized pyrite grains affected by brittle deformation. The As-rich pyrite displays complex compositional zoning, with many of the zones containing small mineral inclusions. Brittle and ductile deformation are present in pyrite and base metal sulfides. Gold occurs as invisible Au in pyrite but also forms discrete grains of electrum. Silver is common as electrum and is present in a range of Ag-sulfosalts. The observed mineral association and generally low base metal grades at TV and Jeff suggests that precious metal enrichment at these deposits occurred at relatively low temperatures (<200°C). The mineral associations at TV and Jeff are distinct from other Au-rich volcanogenic massive sulfide deposits that are generally polymetallic in nature and have formed from hydrothermal fluids having higher temperatures.

TABLE OF CONTENTS

LIST OF FIGURES

LIST OF TABLES

LIST OF ABBREVIATIONS

Mineral abbreviations:

Ag	Native silver
Apy	Arsenopyrite
Ac	Acanthite
Bou	Boulangerite
Ccp	Chalcopyrite
El	Electrum
Fb	Freibergite
Gn	Galena
Mrc	Marcasite
Py	Pyrite
Pyg	Pyrargyrite
Pyh	Pyrrhotite
Qtz	Quartz
Sp	Sphalerite
Usp	Unknown Silver Phase

Other abbreviations:

BSE	Backscattered electron
°C	Degree Celsius
EDS	Energy-dispersive X-ray spectrometry
EMPA	Electron microprobe analysis
FE-SEM	Field emission-scanning electron microscope
g/t	Gram per metric ton
ICP-MS	Inductively coupled plasma-mass spectroscopy
km	Kilometer
keV	Kilo-electron-volt

kV	Kilovolt
LA-ICP-MS	Laser ablation-inductively coupled plasma-mass spectroscopy
m	Meter
μm	Micrometer
mm	Millimeter
Moz	Million ounces
Mt	Million metric tons
myrs	Million years
nA	Nanoampere
%	Percent
s	Second
SEM	Scanning electron microscope
YAG	Yttrium aluminum garnet
VMS	Volcanogenic massive sulfide
wt. %	Weight percent

ACKNOWLEDGEMENTS

I thank my advisor Dr. Thomas Monecke for all his help throughout every aspect of the thesis process. I would not have been able to do this without him. I am also grateful to the members of my thesis committee, Drs. John DeDecker, Ben Frieman, and Katharina Pfaff for their support.

I am indebted to Dr. John DeDecker and everyone at Eskay Mining Corporation for helping me throughout the research project as well as allowing me to work for the company in the 2022 field season and gain valuable industry experience. Completing this thesis would not have been possible without that experience and guidance. Thank you to McKenzee Kocha for help provided during core logging at the camp and sample collection, as well as providing her own samples for me to study.

I am grateful to Dr. Katharina Pfaff and Filip Kasprowicz for their help with the scanning electron microscope. Kelsey Livingston is thanked for making the thin sections. Aaron Bell conducted the electron microprobe analyses and Jay Thompson helped me with the lase ablation-inductively coupled plasma-mass spectrometry analyses. Thank you also to my peers from the past two years for sharing their knowledge and support. I am grateful to my family and friends for their support and encouragement.

This research was supported by Eskay Mining Corporation and Colorado School of Mines. Additional funding was provided by the Society of Economic Geologists Canada Foundation.

CHAPTER 1
INTRODUCTION

Volcanogenic massive sulfide deposits (VMS) are stratiform accumulations of base metal sulfides that have formed at, or immediately below, the seafloor by precipitation from dominantly seawater-derived hydrothermal fluids at temperatures ranging from 250° to 350°C (Franklin et al., 2005; Hannington, 2014). The deposits contain variable concentrations of Cu, Zn, and Pb sulfides. Some deposits are enriched in precious metals making them particularly attractive exploration targets. Commonly, Au-rich deposits contain Au grades exceeding >3.5 g/t and have a total Au endowment of more than ~3 million ounces (Moz; Mercier-Langevin et al., 2011). Controls on precious-metal enrichment in Au-rich VMS deposits are currently not well understood (Fuchs et al., 2019). However, case studies suggest that these deposits may differ widely in metal association and alteration mineralogy (Taube, 1986; Bergman Weihed et al., 1996; Roth et al., 1999; Sherlock et al., 1999; Dubé et al., 2007; Mercier-Langevin et al., 2007; Monecke et al., 2008; Krushnisky et al., 2023), implying that their high Au content cannot be simply attributed to the composition of the hydrothermal fluids or the temperature of sulfide formation. Mercier-Langevin et al. (2011) and Monecke et al. (2014) noted that Au-rich VMS deposits commonly occur in camps suggesting that they may form in specific geodynamic settings or share a common magmatic evolution of the host volcanic successions.

The Jurassic Eskay Creek deposit in the Iskut River region of British Columbia, located about 70 km north of Stewart, is the VMS deposit with the highest precious metal grades (Franklin et al., 2005). Mined from 1994 to 2008, Eskay Creek produced a total of 2.25 million metric tons (Mt) of ore grading 48.9 g/t Au and 2,334 g/t Ag (Meuzelaar, 2015). The deposit is hosted by carbonaceous mudstone overlying a predominately felsic volcanic succession. The ore-forming event overlapped with the onset of a period of intense basaltic volcanism. The volcanic host rocks of Eskay Creek are assigned to the upper Hazelton Group (Roth et al., 1999; Monecke et al., 2005). Although intense exploration ensued within the Iskut River area following the discovery of Eskay Creek in 1989, no other significant VMS deposit was recognized in the region at the time although other Au-rich deposit types occur, including Brucejack (Tombe et al., 2018; Board et al., 2020; McLeish et al., 2021) and Red Chris (Rees et al., 2015; Norris et al.

2023). Compared to other Au-rich VMS deposits worldwide, the occurrence of Eskay Creek as the only significant VMS deposit in the Iskut River area has always been regarded as unusual.

Exploration in the early and mid-1990s resulted in the identification of geochemical anomalies in the TV-Jeff area (Lindsay et al., 2021) (Fig. 2-2). Drilling by Eskay Mining Corp from 2020 to 2022 resulted in a number of high-grade intercepts, including 31.23 g/t Au and 138.1 g/t Ag over 5.08 m in drillhole J20-34 and 2.58 g/t Au and 48.7 g/t Ag over 17.46 m in drillhole TV20-37 (Eskay Mining Corp. Press Release February 2, 2021). Although a resource has not yet been defined for TV-Jeff, recent exploration successes in the Iskut River area now clearly demonstrate that Eskay Creek is not the only Au-rich VMS deposit. In contrast to Eskay Creek, the massive sulfide mineralization at TV-Jeff is hosted by volcanic rocks assigned to the lower Hazelton Group suggesting that more than one stratigraphic position favorable to VMS deposition is present in the Iskut River area (Peterson, 2022), which is not unlike other volcanic successions hosting Au-rich VMS deposits such the Blake River Group of the Abitibi greenstone belt (Mercier-Langevin et al., 2007; McNicoll et al., 2014; Monecke et al., 2017).

The purpose of this thesis is to build upon the study of Peterson (2022), which provided the first detailed descriptions of the volcanic stratigraphy and deposit geology of TV-Jeff. The present study focuses primarily on the ore mineralogy of the TV-Jeff deposits, with particular emphasis being placed on the mineralogical sequestration of the precious metals and the paragenetic relationships of ore-bearing phases. The study furthers the understanding of the localization of Au and Ag enrichment in the ore lenses as grade is highly variable in the pyrite-dominated ores at TV-Jeff. Examination of drill core, as well as detailed petrographic analysis including reflected light microscopy, scanning electron microscopy, automated mineralogy, electron microprobe analysis, and laser ablation-inductively coupled plasma-mass spectroscopy was conducted to study the massive sulfides at TV-Jeff.

CHAPTER 2
GEOLOGIC SETTING

This chapter provides an overview on the geological setting of the TV-Jeff deposits. The regional geological setting along with age relationships are described. In addition, the chapter summarizes the deposit geology including the stratigraphy of the volcanic host rocks and their different modes of emplacement. A brief overview of the current model of ore formation is presented to provide a framework for the discussion of the research on the ore mineralogy of the TV-Jeff deposits.

2.1 Geology of the Stikine Terrane

The TV-Jeff deposits are located in the Iskut River area, about 70 km north of Stewart in British Columbia. The host rocks of the TV-Jeff deposits are part of the allochthonous Stikine Terrane of the northern Canadian Cordillera (Fig. 2-1), which formed away from the western North American margin in an inland arc setting (Marsden and Thorkelson, 1992; Gagnon et al., 2012). The oldest rocks of the polyphase Stikine Terrane are sedimentary and volcanic rocks of the lower Devonian to upper Permian Stikine Assemblage. Rocks of this assemblage do not outcrop in the Iskut River area but have been recognized regionally (MacDonald et al., 1996; Alldrick et al., 2005; Lindsay et al., 2021).

The Stikine Assemblage is unconformably overlain by the Upper Triassic Stuhini Group, which consists primarily of sedimentary rocks, which crop out extensively in the Iskut River area (Fig. 2-2). Dacite, andesite, and bimodal rhyolite-basalt volcanic rocks with an increasing amount of volcaniclastic and siliciclastic rocks occur in the stratigraphically upper parts of the Stuhini Group (Alldrick et al., 2004). The minimum stratigraphic thickness of the Stuhini Group is estimated to be ~3,000 meters (Alldrick et al., 2004).

The Lower to Middle Jurassic Hazelton Group forms a significant proportion of the Stikine Terrane (Tipper and Richards, 1976) and outcrops extensively in the Iskut River area (Fig. 2-2). Previous researchers have proposed that an angular unconformity separates the

Stuhini Group from the overlying volcanic rocks of the Hazelton Group (Alldrick et al., 2004; Nelson and Kyba, 2014; Kyba and Nelson, 2015).

Volcanic and sedimentary rocks of the Hazelton Group represent the last stage of volcanism and arc construction of the Stikine Terrane (Nelson et al., 2013, 2018). It is subdivided into a lower and an upper part. The lower Hazelton Group consists of andesitic to dacitic volcanic rocks, volcaniclastic rocks, and siliciclastic deposits (Gagnon et al., 2012; Prowse et al., 2023). The TV-Jeff deposits are hosted by volcanic rocks of the lower Hazelton Group. The upper Hazelton Group comprises bimodal volcanic rocks and carbonaceous mudstone (Bartsch, 1993; Barrett and Sherlock, 1996; Roth et al., 1999; Monecke et al., 2005; Gagnon et al., 2012). The upper Hazelton Group is host to the Au-rich Eskay Creek deposit (Roth et al., 1999; Sherlock et al., 1999)

During the late Middle Jurassic, the Stikine Terrane amalgamated with the Cache Creek terrane to the east. At the time, the Canadian Cordillera changed from a complex of island arcs, marginal basins, and offshore crustal fragments into an accretionary orogen (Gagnon et al., 2012). Erosion of the composite terrane in the Middle Jurassic to Lower Cretaceous resulted in the deposition of synorogenic, flysch-like, siliciclastic rocks of the Bowser Lake Group (Nelson et al., 2018), which includes greywacke, chert pebble conglomerate, sandstone, and mudstone deposited in a submarine setting (Gagnon and Waldron, 2011). These sedimentary rocks crop out extensively within the 4,900 km^2 Bowser basin to the east and south of the Iskut River area (Fig. 2-2). Mesozoic and Cenozoic plutonic suites intrude all assemblages of the Stikine Terrane (Anderson, 1989; Britton et al., 1989, 1990).

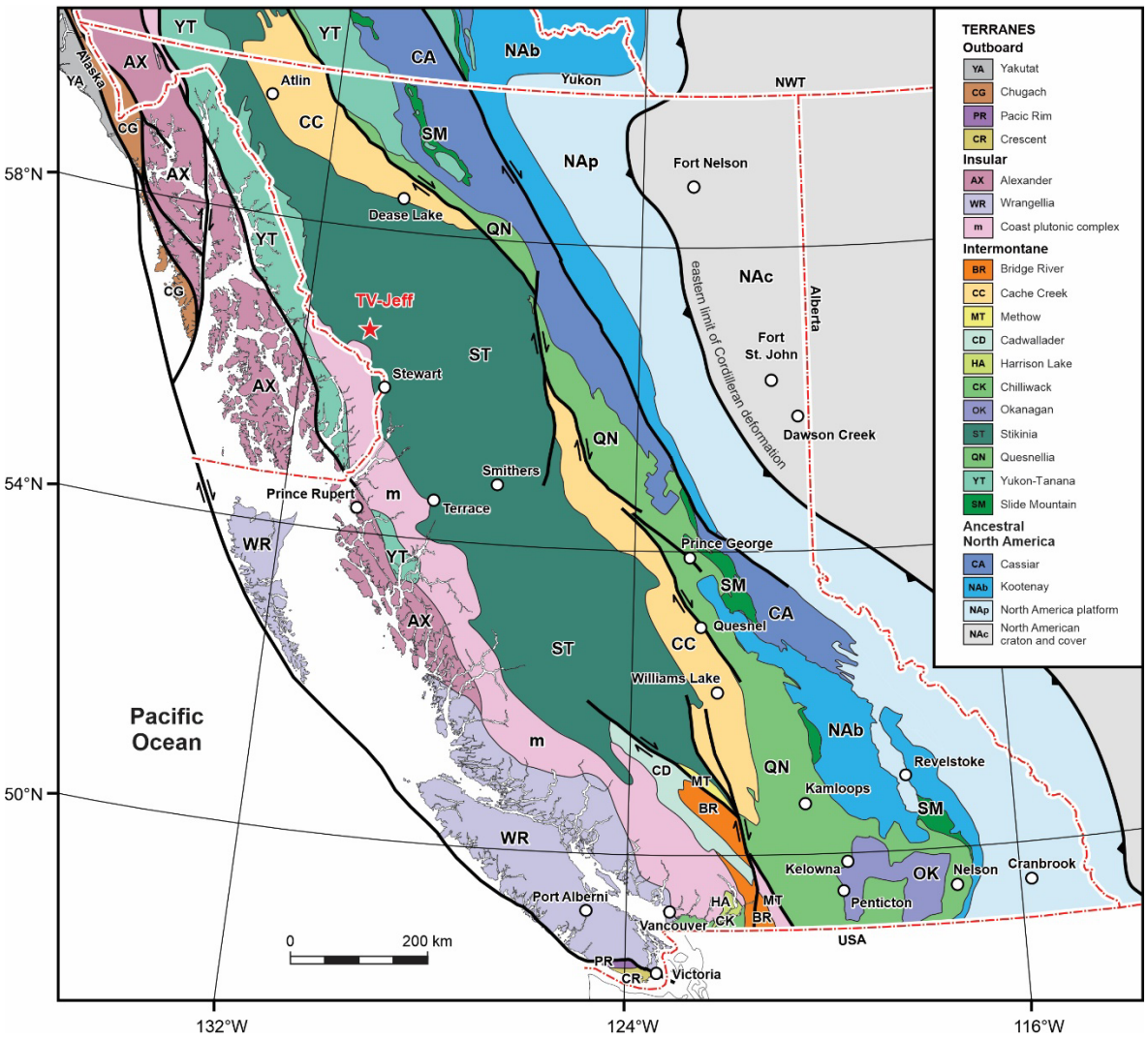

Figure 2-1: Bedrock terrane map of British Columbia (modified from Colpron and Nelson, 2011). The TV-Jeff deposits are located north of Stewart in the Iskut River area at the western margin of the allochthonous Stikine terrane of the northern Canadian Cordillera.

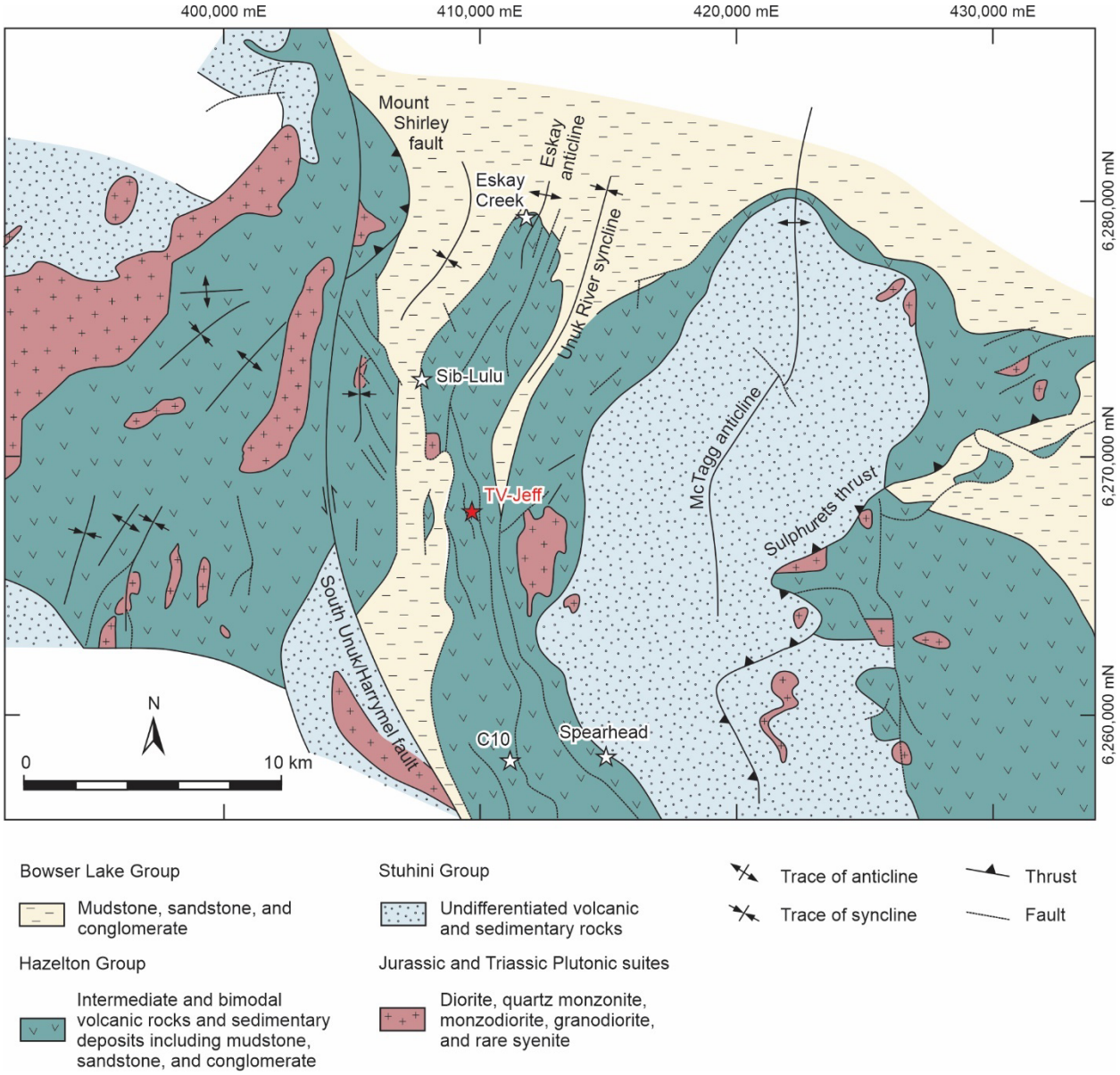

Figure 2-2: Geological map of the Iskut River area and location of the TV-Jeff deposits (modified from MacDonald et al., 1996).

2.2 Stratigraphy of the Hazelton Group

The Hazelton Group is currently divided into a lower and an upper part (Nelson et al., 2018; Lindsay et al., 2021; Peterson, 2022; Prowse et al., 2023). Geochronological and paleontological evidence suggests that the Hazelton Group was emplaced between the Sinemurian and Bajocian from 199–168 Ma, recording ~31 million years (myrs) of sedimentation and volcanism (Fig. 2-3). In comparison to other well-studied, arc-related volcanic successions hosting VMS deposits that show a maximum of ~3–5 myrs range (McNicoll et al., 2014; Mortensen et al., 2015), this is unusually long. This may suggest that possible structural complications are currently not recognized and that what is currently recognized as the Hazelton Group is an assemblage of structurally juxtaposed units or, alternatively, that currently available geochronological constraints are incorrect (T. Monecke, personal communication, 2022).

The lower Hazelton Group is mostly comprised of calc-alkaline to tholeiitic andesitic to dacitic flows, breccias, and tuffs, as well as volcaniclastic units and mudstones (Gagnon et al., 2012; Prowse et al., 2023). It is subdivided into the Jack Formation and the Betty Creek Formation (Fig. 2-3; Nelson et al., 2018; Lindsay et al., 2021). The Jack Formation is the lowermost formation of the lower Hazelton Group and dominated by siliciclastic rocks. It is comprised of conglomerate, sandstones, siltstones, and mudstones (Nelson et al., 2018; Lindsay et al., 2021; Prowse et al., 2023). The Betty Creek Formation represents the upper formation of the lower Hazelton Group (Fig. 2-3; Lindsay et al., 2021; Prowse et al., 2023). The Betty Creek Formation is subdivided into three informal units, referred to as the Unuk River andesite, the Johnny Mountain dacite, and the Brucejack Lake felsic unit (Nelson et al., 2018; Prowse et al., 2023). The Unuk River andesite is the basal unit of the Betty Creek Formation and has a sharp contact with the Jack Formation, representing an abrupt change from a predominantly sedimentary environment to an environment of volcanism and sedimentation during volcanic quiescence (Nelson et al., 2018). The unit is made up of volcaniclastic rocks having an andesitic composition (Nelson et al., 2018). The Johnny Mountain dacite is made up of a succession of massive dacite flow and breccia, as well as peperitic dacite (Nelson et al., 2018; Peterson, 2022; Lindsay et al., 2021; Prowse et al., 2023). The Brucejack Lake felsic unit is a flow-dome complex overlaying the Unuk River andesite (MacDonald, 1993). It consists of porphyritic lava

flows, breccias, and tuffs that are intruded by a flow-banded coherent plagioclase-phyric unit (MacDonald, 1993).

Within the Iskut River area, the upper Hazelton Group is divided into the Spatsizi Formation, the Iskut River Formation, and the Quock Formation (Fig. 2-3; Gagnon et al., 2012; Nelson et al., 2018). The Spatsizi Formation is the basal unit of the upper Hazelton Group and is thought to unconformably overlay the Betty Creek Formation of the lower Hazelton Group (Nelson et al., 2018). The Spatsizi Formation is dominated by volcaniclastic rocks including volcaniclastic conglomerate, sandstone, shale, siltstone, and localized limestone (Nelson et al., 2018; Lindsay et al., 2021). The Iskut River Formation occurs stratigraphically above the Spatsizi Formation (Fig. 2-3). It is a bimodal volcanic succession that contains several intercalated carbonaceous mudstone units (Bartsch, 1993; Barrett and Sherlock, 1996; Roth et al., 1999; Monecke et al., 2005). The Quock Formation overlies the Iskut River Formation, which consists of tuffaceous mudstone (Gagnon et al., 2012).

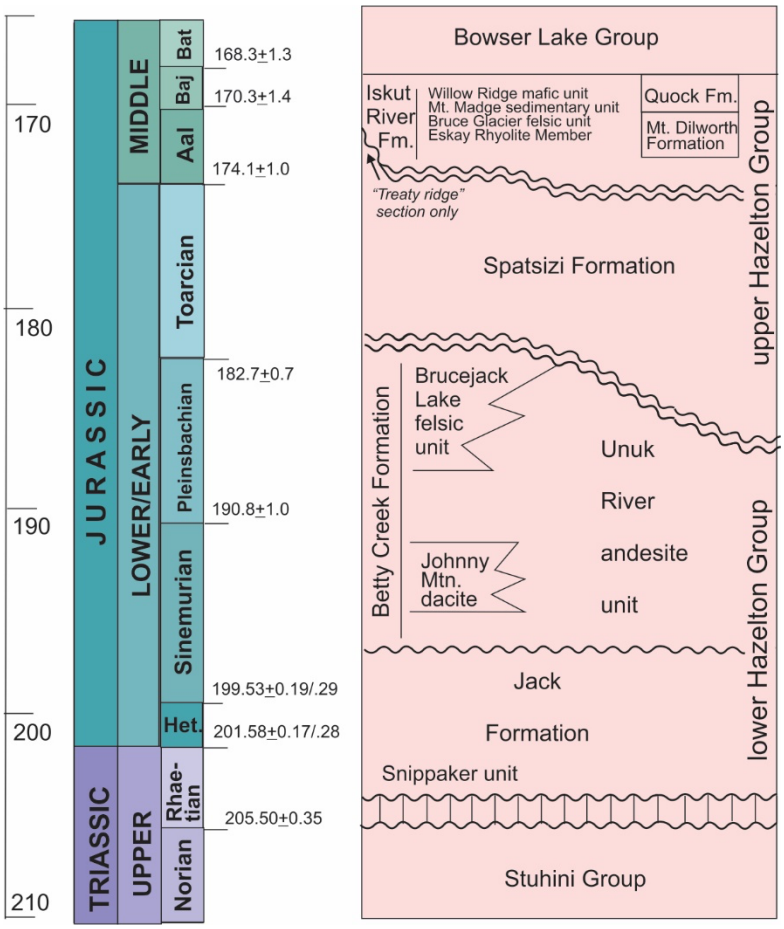

Figure 2-3: Stratigraphy of the Iskut River area and age constraints on stratigraphic units (modified from Nelson et al., 2018).

2.3 Volcanogenic Massive Sulfide Deposits in the Iskut River Area

Eskay Creek is the most famous VMS deposit in the Iskut River area (Fig. 2-2). Mined between 1994 and 2008, Eskay Creek produced a total of 2.25 Mt of ore grading 48.9 g/t Au and 2,334 g/t Ag (Meuzelaar, 2015). The deposit is hosted by the Iskut River Formation. Within the mine area, the host strata are folded into a shallowly north plunging, north-northeast trending, upright, open anticline, referred to as the Eskay anticline (Fig. 2-2). The Eskay Creek deposit occurs on the western limb of the anticline, near the fold closure, and dips gently 30° to 45° to the west. The ore zones are disrupted by several north-northwest to north-northeast trending normal faults (Roth et al., 1999).

The immediate footwall to the stratiform lenses of the Eskay Creek deposit is formed by coherent rhyolite and related volcaniclastic rocks assigned to the Iskut River Formation (Bartsch, 1993; Barrett and Sherlock, 1996; Roth et al., 1999; Monecke et al., 2005; Nelson et al., 2018). The footwall rhyolite has a stratigraphic thickness of approximately 100 m in the mine area (Britton et al., 1990). The footwall rhyolite is locally mineralized hosting discordant zones of stringer veins and disseminated mineralization (Britton et al., 1990; Idziszek et al., 1990; Roth et al., 1999). The main stratiform ore zones, which includes the clastic sulfides of the 21B zone (Britton et al., 1990; Idziszek et al., 1990; Roth et al., 1999), are hosted by a thick package of carbonaceous mudstone. On the western limb of the Eskay anticline, the carbonaceous mudstone interfingers with basalt, which largely was emplaced as sills although pillowed lava flows are also present (Roth et al., 1999; Monecke et al., 2005). The hanging-wall basalt is not recognized at the eastern limb of the Eskay anticline. The basalt is overlain by tuffaceous mudstone currently assigned to the Quock Formation (Gagnon et al., 2012). The youngest strata exposed on both limbs of the Eskay anticline include mudstone, sandstone, and conglomerate of the Bowser Lake Group (Roth et al., 1999).

In addition to Eskay Creek and TV-Jeff, which is described in more detail below, several VMS occurrences have been identified in the Iskut River area (Fig. 2-2). This includes the Sib-Lulu occurrence, which comprise mineralization in the Iskut River Formation, Bruce Glacier felsic unit, Spatsizi Formation, and Betty Creek Formation (J. DeDecker, personal communication, 2023). In 1990, several drill holes intersected stockwork mineralization at Sib-

Lulu. Drillhole DDH 90-30 intersected carbonaceous mudstone of 14 m length assaying 14.4 g/t Au and 1,059.5 g/t Ag containing native gold, pyrargyrite, and arsenopyrite in addition to stibnite and sphalerite (Lindsay et al., 2021).

The C10 occurrence is located 8 km south of TV-Jeff (Fig. 2-2). Drilling in 2021 suggested that this occurrence represents a metamorphosed and strongly deformed VMS system predominated by disseminated sulfides. The highest-grade intercept included 31.10 g/t Au and 4.97 g/t Ag over 1.95 m in drillhole C21-1 (Eskay Mining Corp. Press Release March 15, 2022). The sulfide zone extends for up to 800 m and contains chalcopyrite, pyrite, sphalerite, galena, and arsenopyrite (Lindsay et al., 2021). The dacite and carbonaceous mudstone hosting the mineralization likely forms part of the Betty Creek Formation of the lower Hazelton Group.

The Spearhead occurrence was discovered in 2006 following prospecting on an electromagnetic conductor. Extensive stringer sulfide mineralization is present in outcrops of massive rhyolite intruded into a carbonaceous mudstone forming part of a thick turbidite succession. The host rocks of the Spearhead occurrence have been assigned to the Iskut River Formation. Drilling revealed that the stringers primarily are composed of pyrite containing up to 0.2 wt. % Zn (Lindsay et al., 2021).

2.4 Geology of the TV-Jeff Deposits

The TV and Jeff deposits both lie to the south of Eskay Creek (Fig. 2-2; Lindsay et al., 2021). Unlike Eskay Creek, the TV and Jeff sulfide mineralization is in the lower Hazelton Group (Lindsay et al., 2021; Peterson, 2022; Prowse et al., 2023). The volcanic and sedimentary rocks hosting the deposits are assigned to the Betty Creek Formation although siliciclastic rocks of the Jack Formation have also been encountered during drilling (Peterson, 2022; Prowse et al., 2023). However, the structural versus conformable relationship between the Jack and Betty Creek Formations is poorly understood.

Detailed graphical logging at TV was conducted by Peterson (2022) using drill hole TV20-37. The drill hole consists of various volcanic facies interlayered with hemipelagic mudstone and is characterized by massive and stringer replacement sulfides (Fig. 2-4). There are

two main zones of sulfide mineralization. The first starts at a depth of ~420 m along the core. A scoria breccia and quench fragmented andesite with moderate to intense silicification, chloritization, and sericitization occurs in the stratigraphic footwall to this first sulfide zone (Peterson, 2022). The unit is overlain by volcaniclastic mass flows and mudstone (Peterson, 2022). The mudstone hosts stringer sulfides that transition into massive sulfide at 375 m depth in core (Peterson, 2022). Quench fragmented and autobrecciated andesite with peperitic margins occurs stratigraphically above the massive sulfides. This is followed by a polymictic conglomerate (Peterson, 2022). The volcanic facies then shift from andesitic to dacitic. A series of dacitic units showing various breccia textures before the second sulfide zone is encountered at 225 m depth (Peterson, 2022). The second sulfide zone is much like the first with stringer sulfides in mudstone above and below a massive sulfide unit. The overlying stratigraphy is dominated by andesite breccia and mudstone, with little sulfide mineralization (Peterson, 2022). Although basalt is not present in the drillhole TV20-37, it is present in the TV deposit.

Peterson (2022) also conducted graphic logging of drill hole J20-34 from the Jeff deposit. Much like TV, the drillhole consists of various volcanic facies with intercalated hemipelagic mudstone (Fig. 2-5; Peterson, 2022). The stratigraphically lower part of the hole at 175 m depth consists of a matrix-dominated polymictic conglomerate followed by an in-situ brecciated and flow banded andesite (Peterson, 2022). A polymictic and peperitic breccia made of andesite and dacite with a mudstone matrix cut by sulfide stringers is located stratigraphically above the andesite unit. This unit is then followed by a series of flow banded and variably brecciated andesite (Peterson, 2022). Further up stratigraphy, a volcaniclastic mass flow was noted, which is overlain by another andesitic unit with peperitic margins (Peterson, 2022). Another series of volcaniclastic mass flows occur immediately below and above a sulfide zone located at ~40 m. This sulfide zone overprints a basaltic peperite with sulfide replacement of the mudstone matrix (Peterson, 2022). This unit is overlain by an in-situ brecciated basalt with peperitic bottom and top margins (Peterson, 2022).

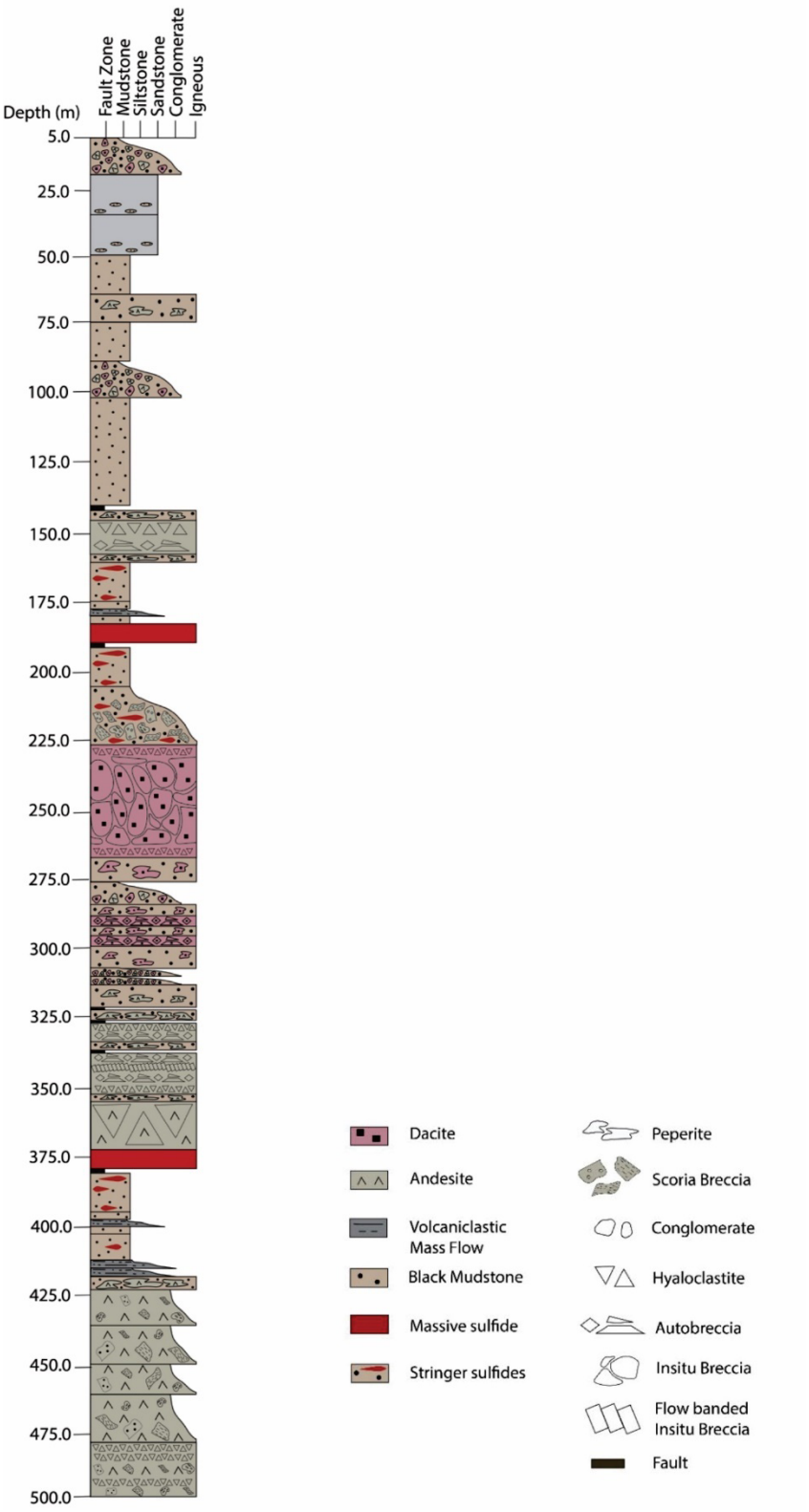

Figure 2-4: Graphic log for drillhole TV20-37 (Peterson, 2022).

Both TV and Jeff contain sulfide minerals as small veinlets or disseminated grains throughout most of the volcanic succession. Figures 2-4 and 2-5 highlight stratigraphic positions that have the highest sulfide mineral abundances. The main differences between TV20-37 and J20-34 are the presence of basalt and lack of dacite in Jeff, as well as the relative depths of the main sulfide zones in both deposits. Despite the differences between the drillholes, TV does have basaltic occurrences and Jeff does have dacitic occurrences (Prowse et al., 2023).

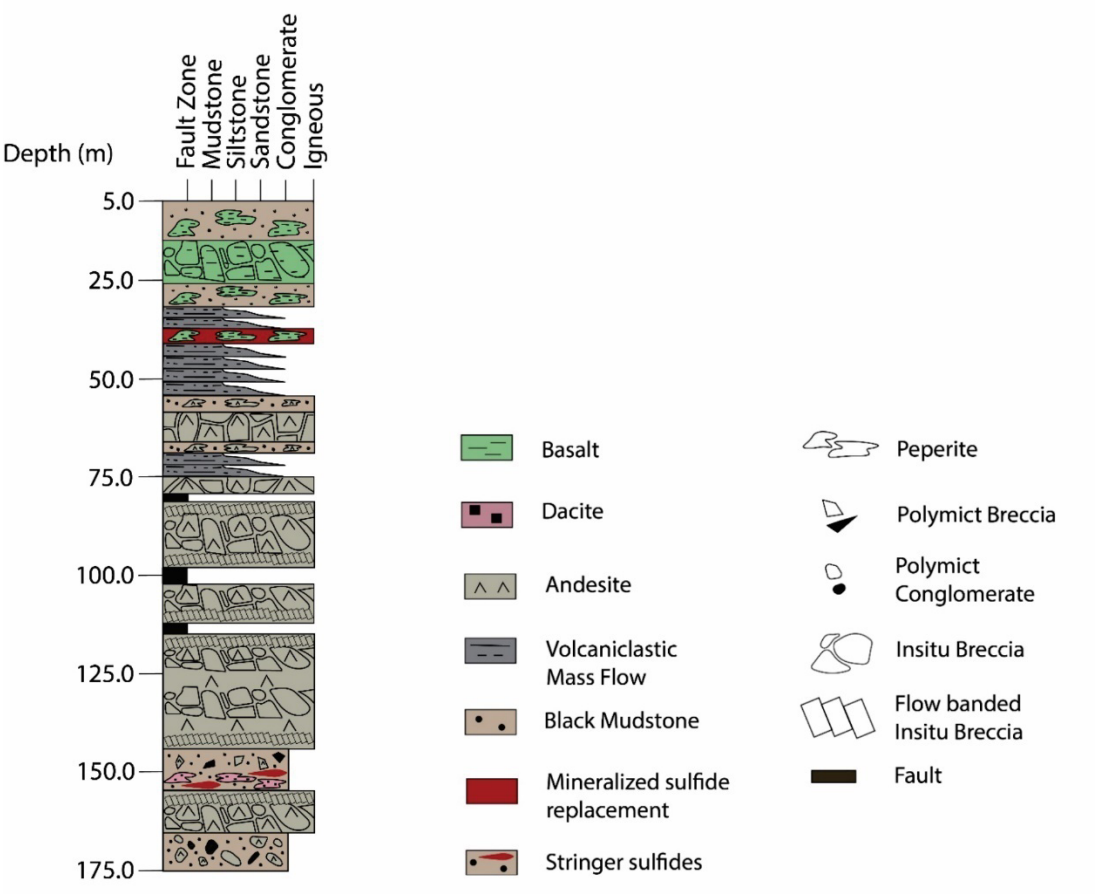

Figure 2-5: Graphic log for drillhole J20-34 (Peterson, 2022).

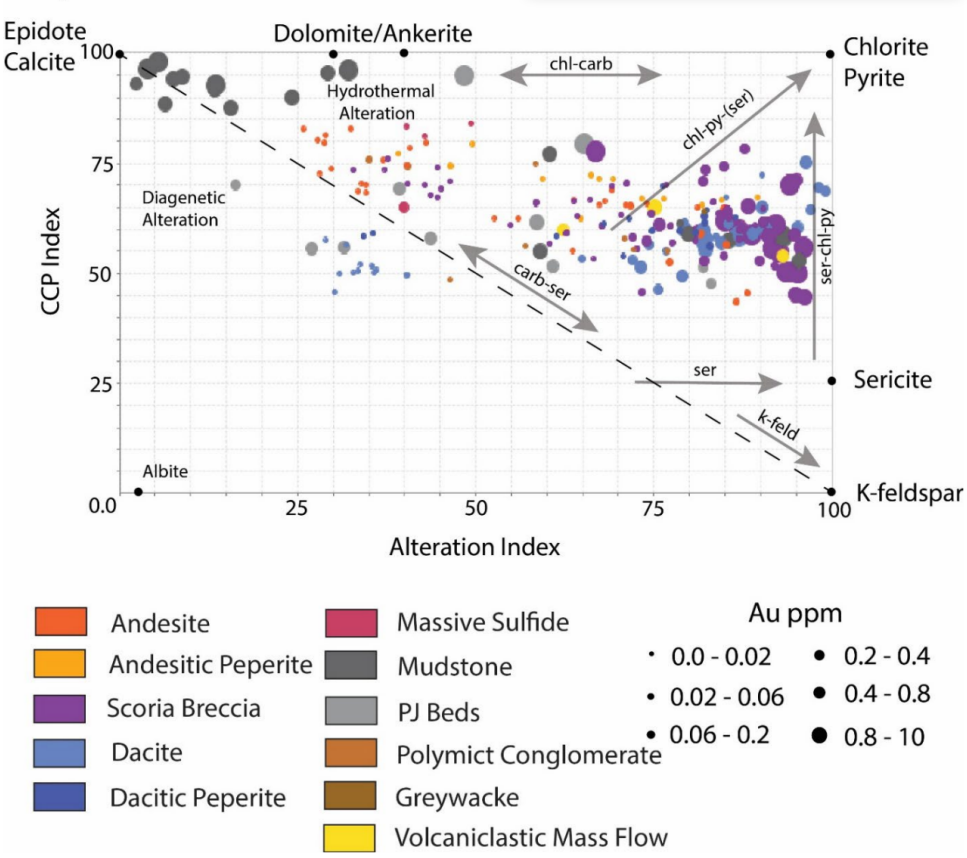

Figure 2-6: Alteration box plot for rocks from the TV deposit (Peterson, 2022).

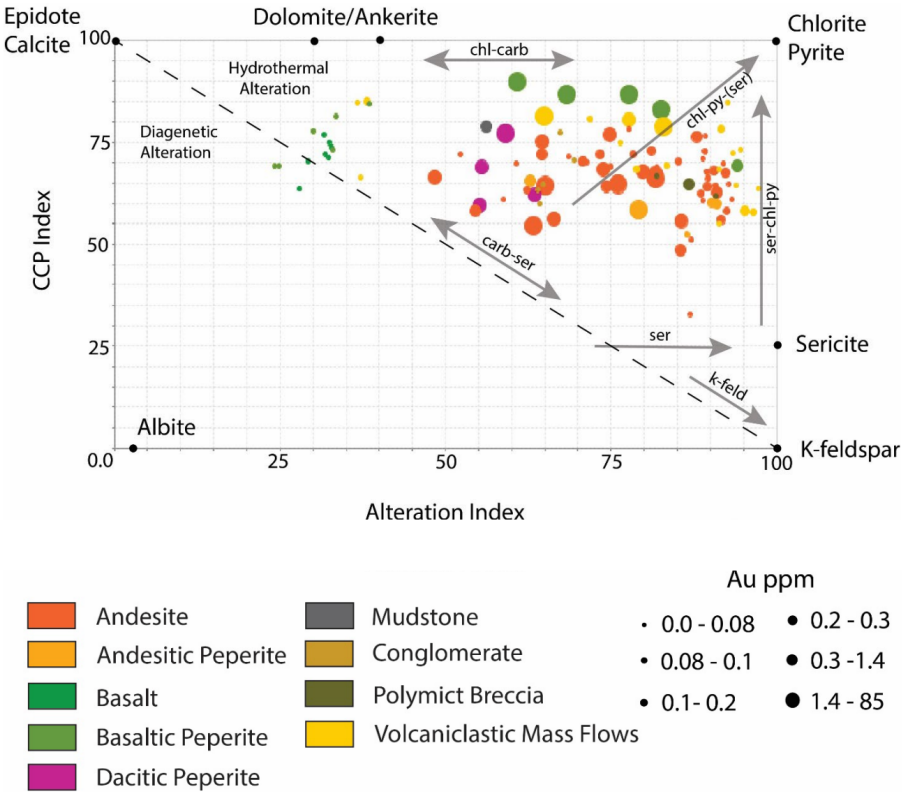

Figure 2-7: Alteration box plot for rocks from the Jeff deposits (Peterson, 2022).

Peterson (2022) showed that elevated Au grades coincide with increased alteration intensities, especially at TV (Figs. 2-6 and 2-7). However, in general host rocks at TV and Jeff are not intensely altered and carbonate alteration appears to be important, which is supported by logging. Intense chlorite alteration indicative for high-temperature alteration has not been recognized at the TV and Jeff deposits. The alteration encountered at TV and Jeff are consistent with low-temperature formation of the mineralization (<250°C; Peterson, 2022; Large et al., 2001).

CHAPTER 3
MATERIALS AND METHODS

As part of this thesis, representative ore samples were collected from the TV-Jeff deposits and analyzed. This section provides a summary of the materials used and describes the various analytical methods employed as part of this research.

3.1 Sampling

A total of 46 samples were collected in the field during the 2022 field season from 19 different drillholes at the TV and Jeff deposits (Fig. 3-1). This includes a total of 25 samples from TV and 21 samples from Jeff (Table 3-1). The samples collected in the field were shipped to Colorado School of Mines and cut into billets. These were used for preparation of standard polished thin sections. In addition to the samples collected as part of this study, 14 thin sections of samples collected by John DeDecker from diamond drill holes TV21-63, TV21-78, and J21-58 were included in this study (Table 3-1).

3.2 Reflected and Transmitted Light Microscopy

Reflected and transmitted light microscopy was performed on Nikon Eclipse LV100POL and Olympus BX53 microscopes at magnifications of 20x, 25x, 40x, 100x, 200x, and 500x. Photomicrographs were taken using a Leica Flexacam C1 cameras attached to both microscopes employing the Leica LAS software package.

3.3 Field Emission-Scanning Electron Microscopy

Representative samples from the TV-Jeff deposits were selected for field emission-scanning electron microscopy (FE-SEM) to study small-scale textural relationships and to image chemical zoning. The FE-SEM analyses were performed on a TESCAN MIRA3 LMH Schottky FE-SEM at the Mineral and Materials Characterization Facility in the Department of Geology and Geological Engineering at Colorado School of Mines. The FE-SEM is equipped with a TESCAN motorized retractable annular, single-crystal YAG backscattered electron (BSE) detector and a Bruker XFlash 6|30 silicon drift detector for energy-dispersive X-ray spectrometry (EDS). The BSE imaging and EDS analyses were performed at 20 kV acceleration voltage, a

working distance of 10 mm and a beam intensity of 11. BSE images were collected at a scanning speed of seven.

3.4 Bright-Phase Automated Mineralogy

Bright-phase searches were conducted at the Mineral and Materials Characterization Facility in the Department of Geology and Geological Engineering at Colorado School of Mines. Two thin sections from drillhole TV21-63 were used. The bright phase searches were performed using a TESCAN-VEGA-3 scanning electron microscope and the TIMA analytical software suite. Two energy dispersive X-ray spectrometers acquired spectra at 1.5 μm step sizes, with an acceleration voltage of 25 keV, and a beam intensity of 16. The scans were set to brightness levels used to target Au- and Ag-bearing minerals within the samples. A high-resolution BSE map was produced and used to navigate to individual grains on the FE-SEM for mineral analyses.

3.5 Electron Microprobe

Electron microprobe (EMP) work was performed on February 13–15, 2023 at the Electron Microprobe Laboratory at the University of Colorado, Boulder, using a JEOL 8230 electron microprobe equipped with five wavelength dispersive X-ray spectrometers. Data was collected with a 2 μm beam diameter, a 5 nA beam current, and an accelerating voltage of 15 kV. The suite of elements that were analyzed included Au, Ag, As, Pb, S, Sb, Cu, Fe, and Zn. The on-peak count time was 20 seconds for Au and 10 seconds for Ag, As, Pb, S, Sb, Cu, Fe, and Zn. The off-peak count time was 20 seconds for Au and 10 seconds for Ag, As, Pb, S, Sb, Cu, Fe, and Zn. Analyses were performed using Kα X-ray emission lines for S, Cu, Fe, and Zn; Lα lines for Au, Ag, As, and Sb; and the Mα lines for Pb. All analyses were performed with large area LIFL (Au, Cu, Fe, and Zn), PETL (Ag, Pb, S and Sb), or TAP (As) analyzing crystals. Standards used included pure metals for Ag and Au; arsenopyrite for As; chalcopyrite for Cu and Fe; galena for Pb; sphalerite for S and Zn; and stibnite for Sb.

3.6 Laser Ablation-Inductively Coupled Plasma-Mass Spectroscopy

Laser ablation-inductively coupled plasma-mass spectroscopy (LA-ICP-MS) analysis was conducted on pyrite from TV-Jeff on January 30–31, 2023, at the U.S. Geological Survey in

Lakewood using a Teledyne Analyte-110 system coupled to an Agilent 8900 ICP-MS. Data were obtained using a spot size of 25 μm and an ablation duration of 30 s. Calibration was conducted using the external synthetic sulfide reference material MASS-1 (Wilson et al., 2002). An average Fe content of 46% (based on EMPA data) was used as an internal standard for all concentration calculations using the methods outlined by Longerich et al. (1996). Minor and trace element analyses were performed for Ag, Al, As, Au, Ba, Bi, Cd, Cu, Hg, K, La, Mg, Mn, Mo, Na, Ni, Pb, Sb, Se, Sn, Sr, Tl, Y, Zn, and Zr. Only element concentrations that were typically above the limit of detection are listed in this contribution. During data processing, the time-resolved LA-ICP-MS signals were carefully inspected to eliminate data from analytical spots that intersected inclusions. Consequently, trace element concentrations reported in the present study are viewed as being related to the incorporation of these elements in the pyrite structure. In total, 140 spots on 29 grains contained in six samples from different drillholes at TV-Jeff were analyzed.

Table 3-1: List of samples from the TV-Jeff deposits investigated in this study.

Drillhole	From (m)	To (m)	Sample
TV21-49	33.15	33.36	TV21-49-1
TV21-49	34.24	34.48	TV21-49-2
TV21-52	69.56	69.61	TV21-52-1
TV21-52	71.40	71.61	TV21-52-2
TV21-53	46.52	46.63	TV21-53-1
TV21-53	46.63	46.74	TV21-53-2
TV21-54	281.54	281.96	TV21-54-1
TV21-54	282.49	282.86	TV21-54-2
TV21-54	283.54	283.69	TV21-54-3
TV21-56	40.58	40.80	TV21-56-1
TV21-56	41.38	41.46	TV21-56-2
TV21-56	42.22	42.33	TV21-56-3
TV21-63	10.13	10.49	TV21-63-10.13*
TV21-63	12.47	12.61	TV21-63-12.47*
TV21-63	28.60	28.75	TV21-63-1
TV21-63	28.80	28.95	TV21-63-28.8*
TV21-63	28.90	28.95	TV21-63-28.9*
TV21-63	31.28	31.46	TV21-63-31.28*
TV21-78	31.93	38.07	TV21-78-31.93*
TV22-84	184.51	184.65	TV22-84-1
TV22-86	186.84	187.00	TV22-86-1
TV22-86	294.34	294.42	TV22-86-2
TV22-87	143.13	143.26	TV22-87-1
TV22-89	121.75	121.88	TV22-89-1
TV22-89	178.23	178.51	TV22-89-2
TV22-95	148.50	148.62	TV22-95-1
TV22-95	153.15	153.30	TV22-95-2
TV22-95	166.36	166.48	TV22-95-3
TV22-95	166.55	166.69	TV22-95-4
TV22-95	189.80	189.96	TV22-95-5
TV22-95	195.66	195.81	TV22-95-6

Table 3-1 (continued)

Drillhole	From (m)	To (m)	Sample
J20-33	58.00	58.36	J20-33-1
J20-33	59.62	59.84	J20-33-2
J20-33	61.41	61.65	J20-33-3
J21-46	27.67	27.88	J21-46-1
J21-47	227.19	228.18	J21-47-1
J21-51	326.90	326.97	J21-51-1
J21-51	332.06	332.22	J21-51-2
J21-53	9.61	9.81	J21-53-1
J21-58	26.14	26.30	J21-58-26.14*
J22-104	171.54	171.78	J22-104-1
J22-105	259.00	259.25	J22-105-1
J22-105	260.35	260.57	J22-105-2
J22-122	117.07	117.27	J22-122-1
J22-122	118.20	118.37	J22-122-2
J22-122	126.72	127.19	J22-122-3
J22-122	129.20	129.33	J22-122-4
J22-122	132.84	133.27	J22-122-5
J22-122	135.18	135.28	J22-122-6
J22-122	172.63	172.73	J22-122-7
J22-122	172.81	172.95	J22-122-8
J22-122	173.54	173.71	J22-122-9
J22-122	189.75	189.92	J22-122-10

Notes: * = Thin sections provided by John DeDecker

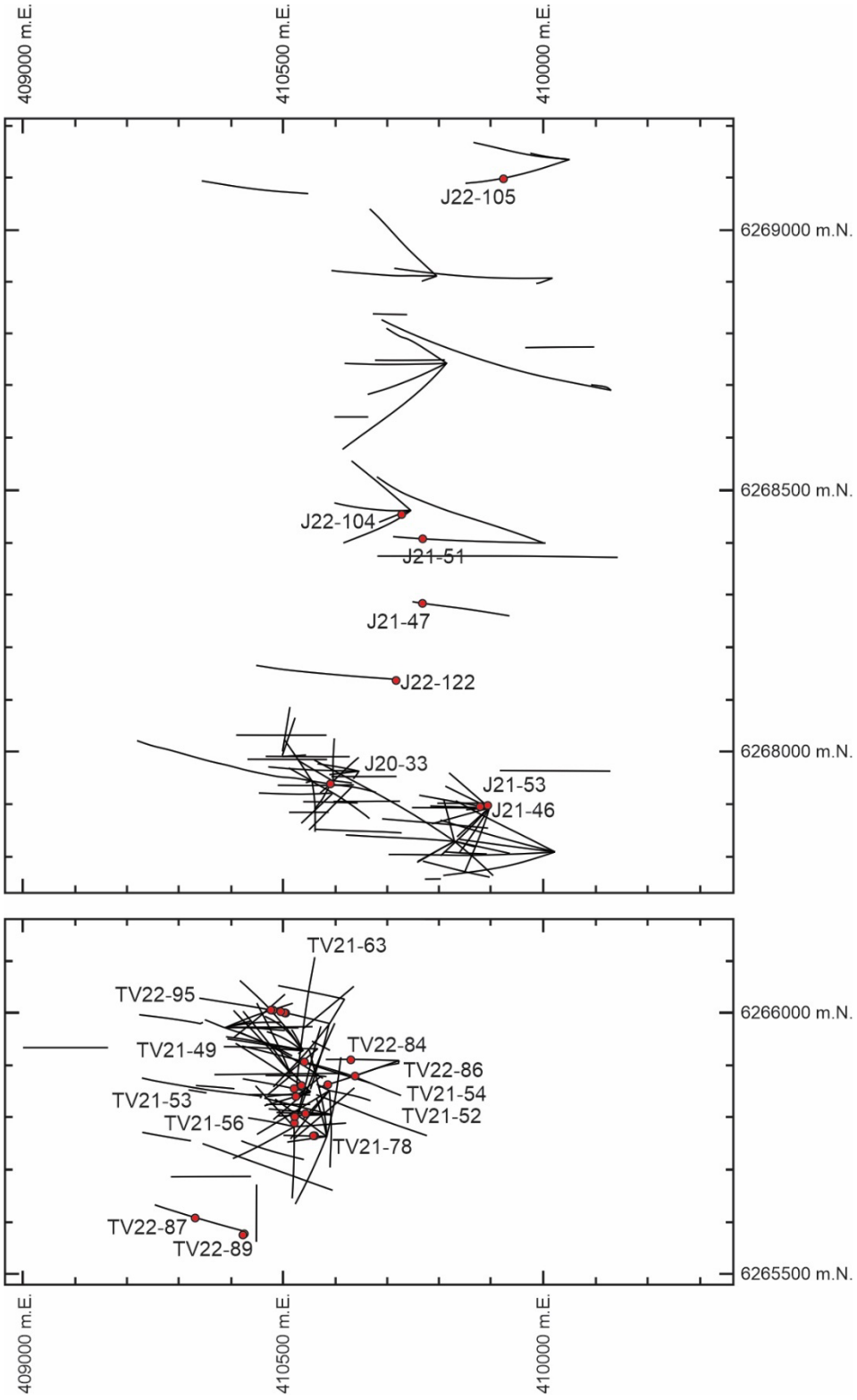

Figure 3-1: Drill plan of the TV and Jeff deposits and locations of samples collected for this study.

CHAPTER 4
RESULTS

Reflected light microscopy, bright-phase automated mineralogy, as well as BSE imaging and EDS point analyses on the SEM were conducted as part of the petrographic analyses of this study. These methods allowed the identification of the ore minerals present and the development of a paragenetic model. Electron microprobe analysis was used to obtain quantitative geochemical analyses on certain minerals. LA-ICP-MS was used to understand the localization of Au and Ag in pyrite from the TV-Jeff deposits.

4.1 Major Ore Mineralogy

Pyrite is the most abundant sulfide at the TV and Jeff deposits. Several distinct pyrite types were identified that appear to have formed at different paragenetic stages. Framboidal pyrite appears to be the paragenetically earliest pyrite type (Fig. 4-1A). The framboidal pyrite is rarely larger than 25 μm in diameter and is characterized by its rounded shapes. The second type of pyrite is subhedral to euhedral and occurs with and without the framboidal pyrite. This is the most abundant form of pyrite. These grains commonly are inclusion-rich containing other sulfide and sulfosalt minerals. This pyrite commonly exhibits moderate to strong deformation textures (Figs. 4-1 and 4-2). Pyrite porphyroblasts are common and are euhedral. Brittle deformation of the pyrite is common, and pyrite porphyroblasts are commonly rotated into the foliation (Figs. 4-1 and 4-2). Lastly, there is pyrite and marcasite that displays birds-eye texture (Fig. 4-1B). It only occurs with pyrrhotite and shows a pyrrhotite breakdown reaction resulting in the formation of pyrite and marcasite.

Pyrrhotite, sphalerite, chalcopyrite, and galena are common in the sulfide veins and massive sulfides at the TV and Jeff deposits. These sulfides always occur with pyrite, whether it is between pyrite grains, in fractures, or along pyrite grain boundaries (Figs. 4-1 and 4-2). Galena, sphalerite, and chalcopyrite form a matrix surrounding pyrite porphyroblasts suggesting that they have experienced ductile deformation (Fig. 4-2E, F). Chalcopyrite is less abundant than galena, sphalerite, and pyrrhotite. It most commonly forms irregular, blebby aggregates within sphalerite, forming chalcopyrite disease (Fig. 4-1D). Pyrrhotite and galena can also be found

within sphalerite as inclusions, although they are much less frequent in this form than chalcopyrite (Fig. 4-1D). Sphalerite and chalcopyrite are also in the pyrite mineral fish (Fig. 4-2D).

Electrum is abundantly present and can be identified in reflected light microscopy. It occurs along the grain boundaries of pyrite and infills fractures within this mineral (Fig. 4-1E, F). It occurs with arsenopyrite, chalcopyrite, freibergite, galena, and sphalerite (Fig. 4-1E, F). Most commonly, electrum occurs with galena (Fig. 4-1E). The characteristics are further described based on SEM analysis in the following section.

4.2 Accessory Ore Mineralogy

Bright-phase scans were conducted on sample TV21-63-28.8 taken from the interval with assay grades of 2,640 ppm Ag and 3.75 ppm Au. One of the bright-phase scans is shown in Figure 4-3, with the Ag-bearing accessory ore minerals highlighted. The scan shows that the Ag-bearing phases form fracture fills crosscutting the silicate matrix and occur in association with other sulfide phases. The bright phase scans were used to navigate to the individual grains on the SEM to allow semiquantitative analysis of the phases by EDS.

Scanning electron microscopy and EDS point analyses were used to further determine the ore mineralogy, as well as their textures and paragenesis. The main use of the EDS system was to determine the composition of the Au- and Ag-bearing minerals. The minerals observed in reflected light microscopy and scanning electron microscopy are listed in Table 1.

Electrum is the only Au-bearing phase identified using optical microscopy and EDS for the TV and Jeff deposits. Electrum occurs in veinlets and grain boundaries of pyrite (Figs. 4-1E, F and 4-4). The grains observed range from about 1 to 50 μm in size. Most commonly, electrum occurs with galena (Fig. 4-4), as well as along arsenic growth zones in pyrite (Fig. 4-8).

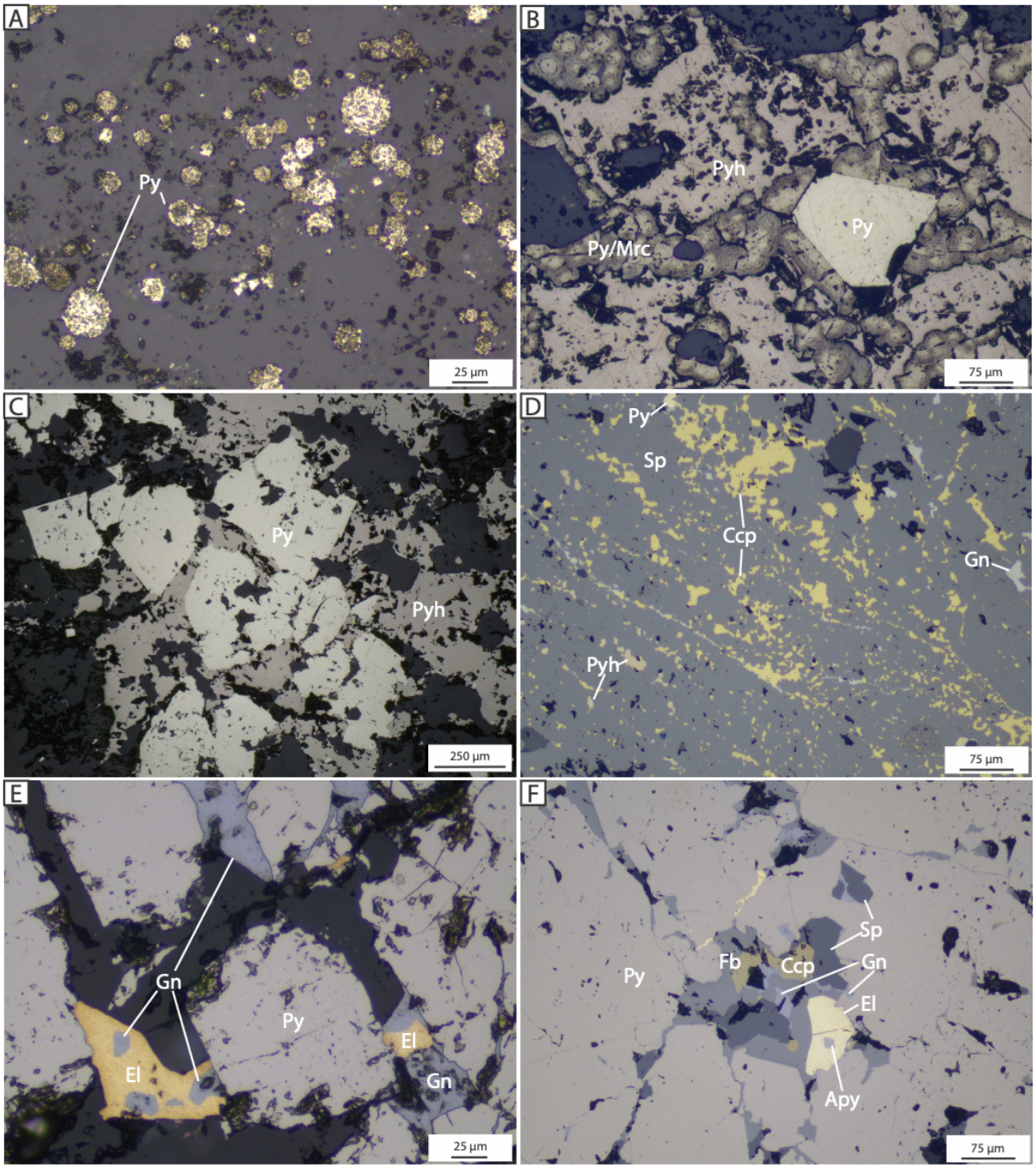

Figure 4-1: Photomicrographs of ore minerals in reflected light from the TV and Jeff deposits. (A) Framboidal pyrite. Sample TV21-53-1. (B) Late-stage pyrite and marcasite showing bird's-eye texture in pyrrhotite surrounding pyrite porphyroblast. Sample TV21-63-10.13A. (C) Pyrite porphyroblast surrounded by pyrrhotite. Sample J22-122-4. (D) Chalcopyrite disease in sphalerite. Sample J22-122-8. (E) Electrum and galena in fractures between pyrite. Sample J20-33-2. (F) Aggregate of arsenopyrite, chalcopyrite, electrum, freibergite, galena, and sphalerite within pyrite. Sample TV21-53-1. Abbreviations: Apy=arsenopyrite, Ccp=chalcopyrite, El=electrum, Fb=freibergite, Gn=galena, Mrc=marcasite, Py=pyrite, Pyh=pyrrhotite, and Sp=sphalerite.

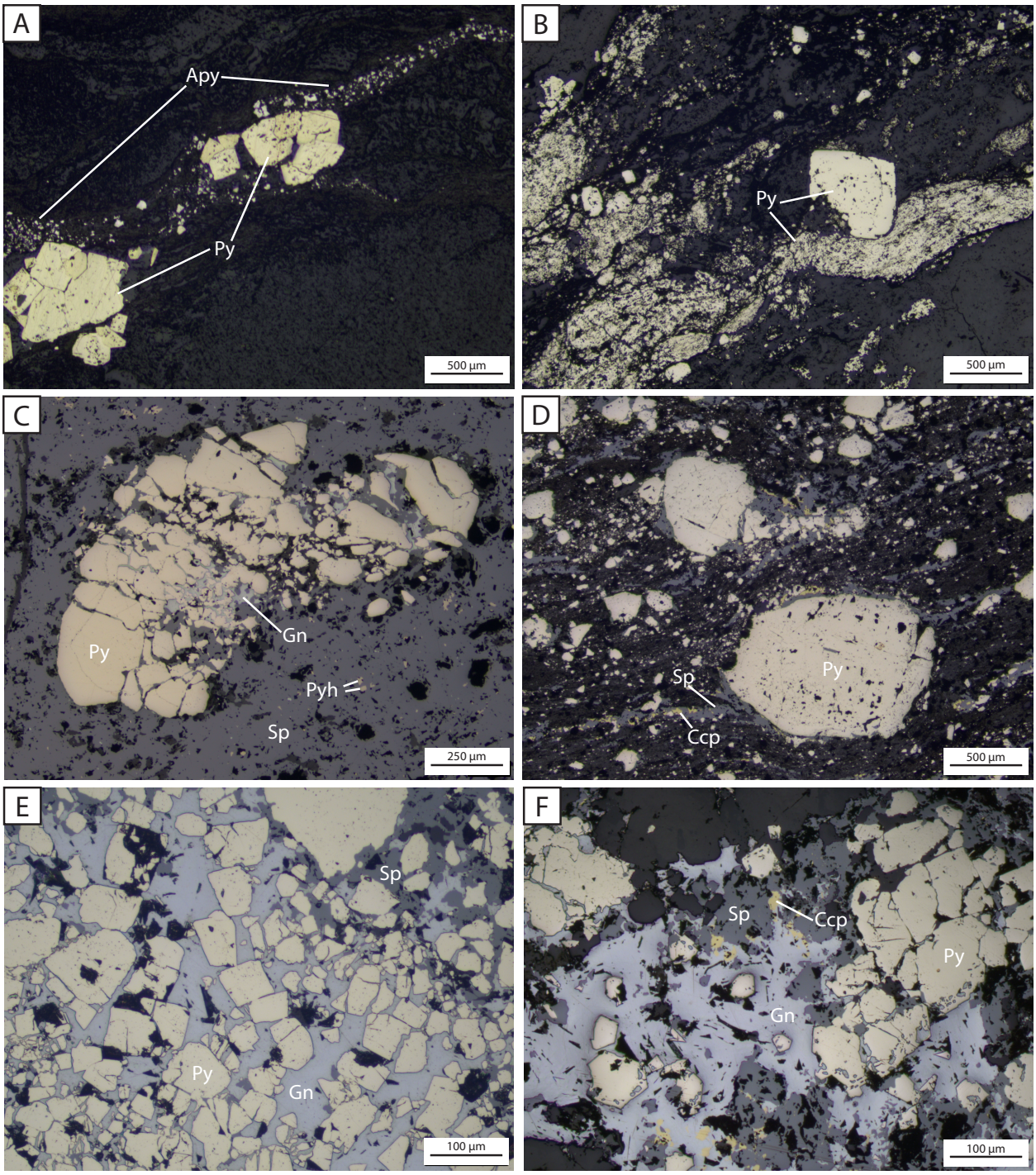

Figure 4-2: Photomicrographs of deformed and recrystallized pyrite in reflected light from the TV and Jeff deposits. (A) Recrystallized pyrite and arsenopyrite. Sample J21-58-26.14A. (B) Recrystallized and deformed pyrite. Sample TV21-56-3. (C) Brittle deformation of pyrite. Sample J22-122-7. (D) Deformed pyrite showing dextral shear. Sample J21-51-2. (E) Pyrite porphyroblasts in a ductile matrix of galena. Sample J22-122-9. (F) Pyrite porphyroblasts in a ductile matrix of galena, sphalerite, and chalcopyrite. Sample J22-122-9. Abbreviations: Apy=arsenopyrite, Ccp=chalcopyrite, Gn=galena, Py=pyrite, Pyh=pyrrhotite, and Sp=sphalerite.

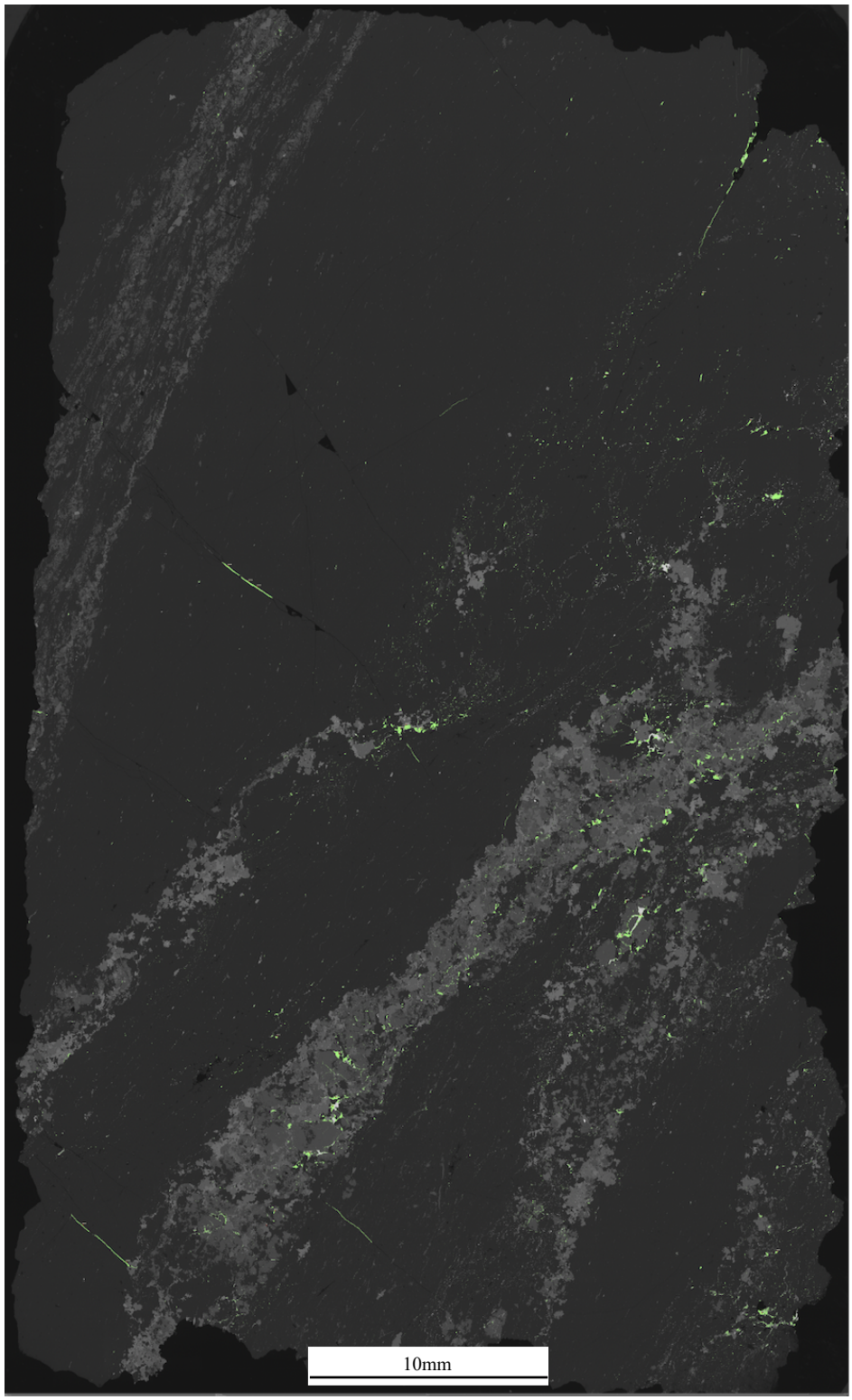

Figure 4-3: High-resolution bright-phase scan of sample TV21-63-28.8. Silver-bearing phases are highlighted in green.

In addition to electrum, a range of Ag-bearing minerals have been identified at the TV and Jeff deposits (Table 4-1). The most abundant Ag-bearing minerals are freibergite and pyrargyrite. Freibergite mostly forms irregularly shaped aggregates, both separated from other sulfides and sulfosalts and associated with them (Fig. 4-5). Freibergite is also present as inclusions along growth zones in pyrite, similar to electrum (Fig. 4-8). Pyrargyrite commonly forms veinlets (Fig. 4-3) or occurs along fractures crosscutting pyrite and sphalerite (Fig. 4-5). Acanthite occurs as masses, as does native silver (Fig. 4-5B, F). The bladed texture of native silver is less defined than that of acanthite, and the native Ag blades are only readily visible on the rims of the grains (Fig. 4-5B). Native silver also occurs in masses of greater than 500 μm width, while displaying a black rim under SEM that separates it from other sulfides and sulfosalts (Fig. 4-5A). Diaphorite was detected once through EDS spot analysis. There is also an unknown phase containing Ag, Sb, and S (Fig. 4-5E).

Other minerals identified by SEM include boulangerite as well as arsenopyrite. Boulangerite displays a bladed texture, and it is also seen rimming pyrite and Ba-rich feldspar (Fig. 4-5C). Arsenopyrite is euhedral and is seen in clusters of Ag-bearing sulfides and sulfosalts, within electrum and with sulfosalts (Figs. 4-1 and 4-5A, C). Bournonite was not found in any samples from this study but was documented by Peterson (2022).

Table 4-1: Ore minerals identified at the TV-Jeff deposits.

Mineral	**Formula**
Acanthite	Ag_2S
Arsenopyrite	AsFeS
Boulangerite	$Pb_5Sb_4S_{11}$
Bournonite	$PbCuSbS_3$
Chalcopyrite	$CuFeS_2$
Diaphorite	$Ag_3Pb_2Sb_3S_8$
Electrum	(Au,Ag)
Freibergite	$(Ag,Cu,Fe)_{12}Sb_4S_{13}$
Galena	PbS
Marcasite	FeS_2
Miargyrite	$AgSbS_2$
Native silver	Ag
Pyrite	FeS_2
Pyrargyrite	Ag_3SbS_3
Pyrrhotite	FeS
Sphalerite	(Zn,Fe)S
Stephanite	Ag_5SbS_4
Unknown Phase	(Ag,Sb,S)

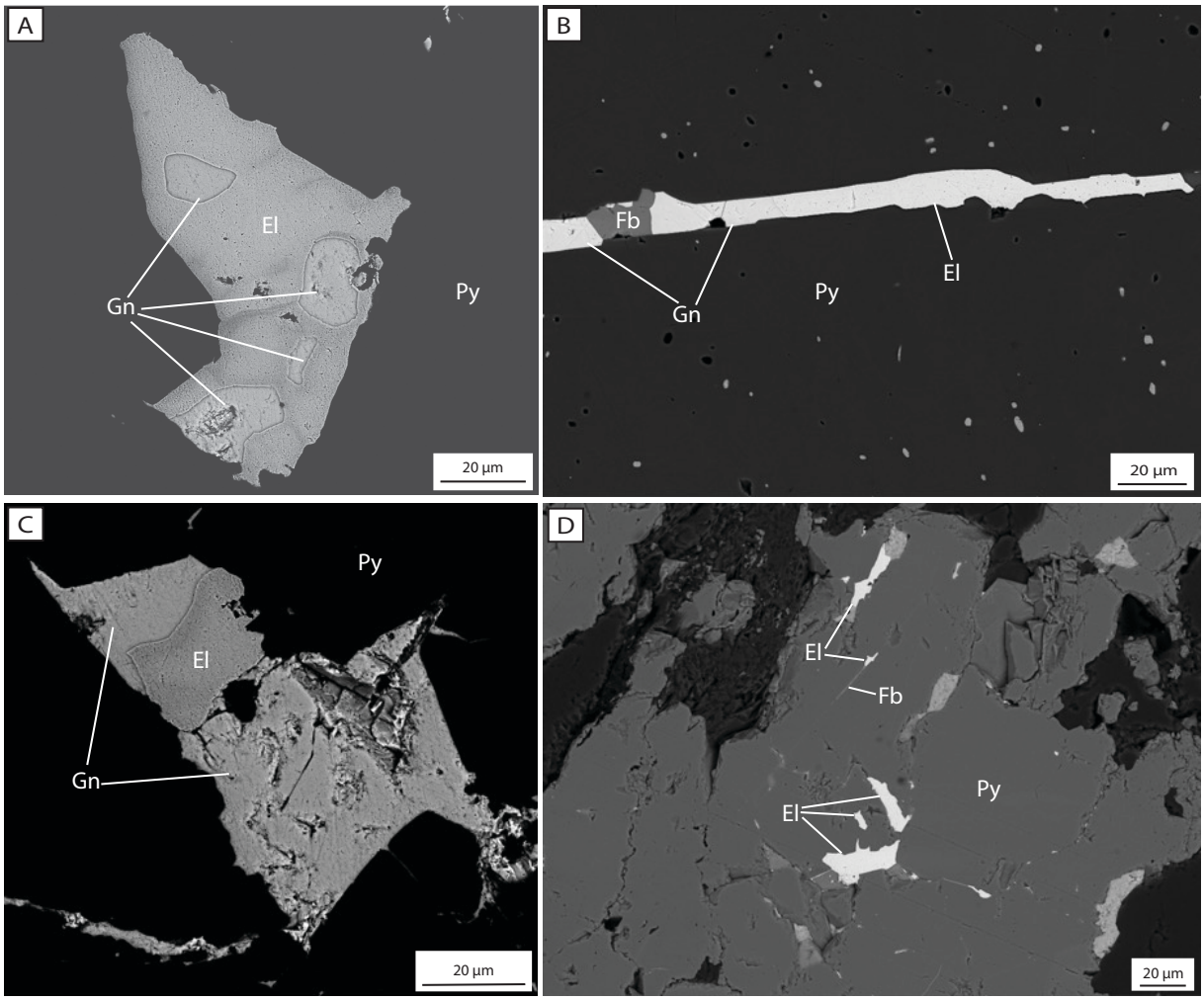

Figure 4-4: Backscattered electron images showing the occurrence of electrum. (A) Electrum and galena inclusions in pyrite. Sample J20-33-1. (B) Veinlet of electrum, freibergite, and galena crosscutting pyrite. Sample TV21-53-1. (C) Electrum and galena surrounded by pyrite. Sample J20-33-1. (D) Electrum and freibergite inclusions within pyrite grain. Sample TV21-52-1. Abbreviations: El=electrum, Fb=freibergite, Gn=galena, and Py=pyrite.

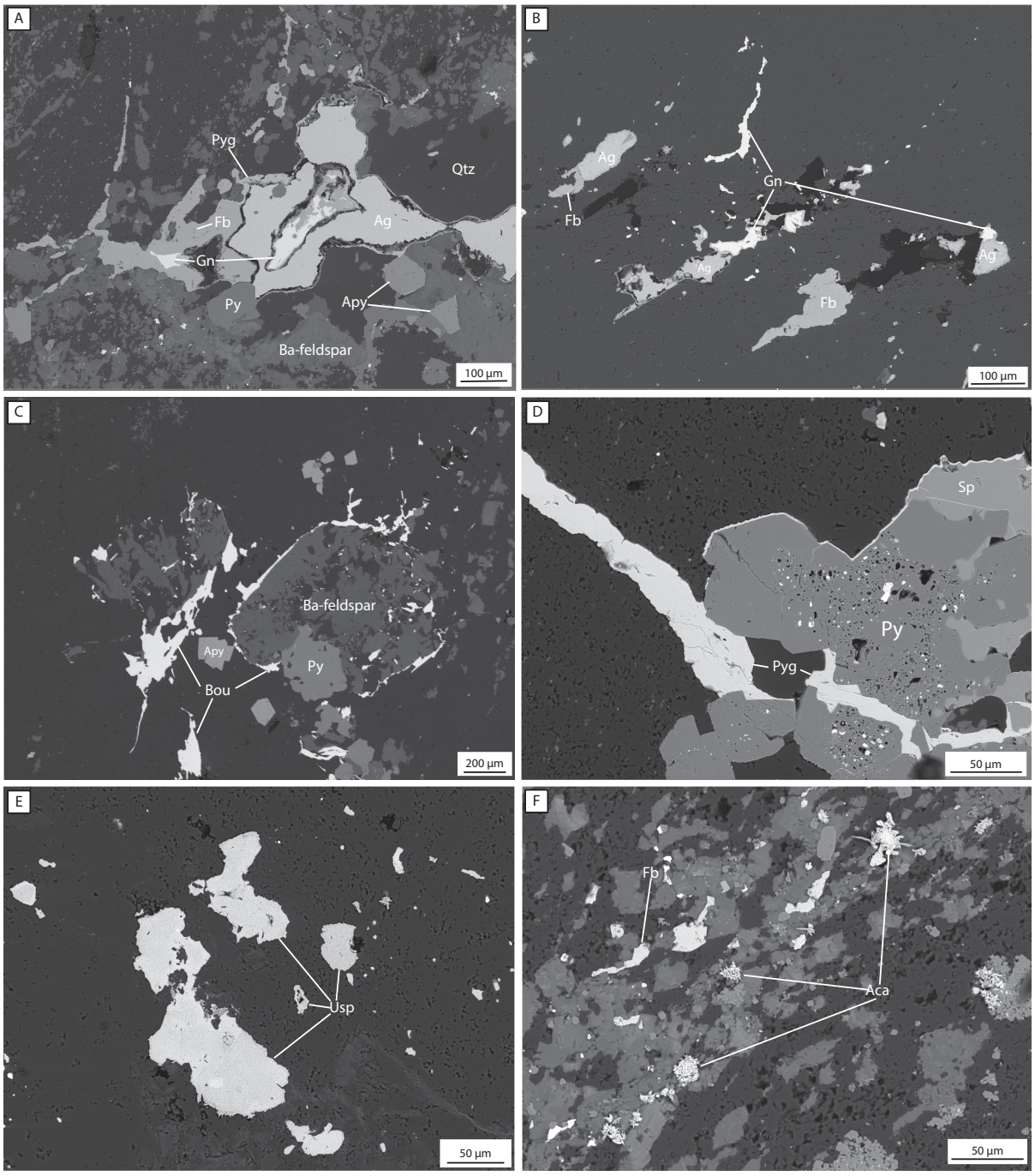

Figure 4-5: BSE images of Ag and Pb-bearing sulfides and sulfosalts. (A) Arsenopyrite, freibergite, galena, native silver, pyrargyrite, and pyrite with Ba-feldspar and quartz. Sample TV21-63-28.9. (B) Freibergite, galena, and native silver. Sample TV21-63-28.9. (C) Arsenopyrite, boulangerite, and pyrite with Ba-feldspar. Sample TV21-63-31.28. (D) Pyrargyrite crosscutting sphalerite and pyrite. Sample TV21-63-28.9. (E) Unknown Ag-bearing phase. Sample J21-58-26.14. (F) Acanthite and freibergite. Sample TV21-63-28.9. Abbreviations: Ac=acanthite, Ag=native silver, Apy=arsenopyrite, Bou=boulangerite, Fb=freibergite, Gn=galena, Py=pyrite, Pyg=pyrargyrite, Qtz=quartz, Usp = unknown silver phase, and Sp=sphalerite.

4.3 Composition of Precious Metal-Bearing Ore Minerals

Electron microprobe analysis was used to obtain quantitative geochemical analyses on certain ore phases, including electrum, freibergite, pyrargyrite, native Ag, boulangerite, and an unknown Ag-bearing phase.

Phase analysis revealed that the distribution of Au and Ag in electrum grains is fairly uniform, with Au concentrations ranging from 56.31 to 62.86 wt. % and Ag concentrations ranging from 38.59 to 44.17 wt. % (n=6; Fig. 4-6; Table 4-2). This corresponds to millesimal fineness values of 560 to 620.

The compositional variations of Ag-bearing phases freibergite, pyrargyrite, native Ag, and the unknown Ag-bearing phase are plotted in the ternary diagram of Figure 4-7. The endmember compositions of common Ag-bearing phases are given for comparison (Voudouris et al., 2011). The plot shows that grains of the tetrahedrite group analyzed can be classified as freibergite due to their elevated Ag contents. There are two main clusters of freibergite that differ in the amount of Sb contained. The pyrargyrite point analyses tested from the TV and Jeff samples have more Ag than the standard endmember (Fig. 4-7).

Microprobe analysis was also conducted on an unknown Ag-bearing phase that predominantly consists of Ag, with concentrations ranging from 79.26 to 90.25 wt. % Ag. The Sb concentration of this phase varies from 3.40 to 14.97 wt. % and the S content is between 1.80 and 3.56 wt. % (Table 4-3). Boulangerite was also analyzed by the electron microprobe. The compositions of the different boulangerite grains are relatively uniform, with representative analyses given in Table 4-4. Some boulangerite analyses contain minor Ag (Table 4-4).

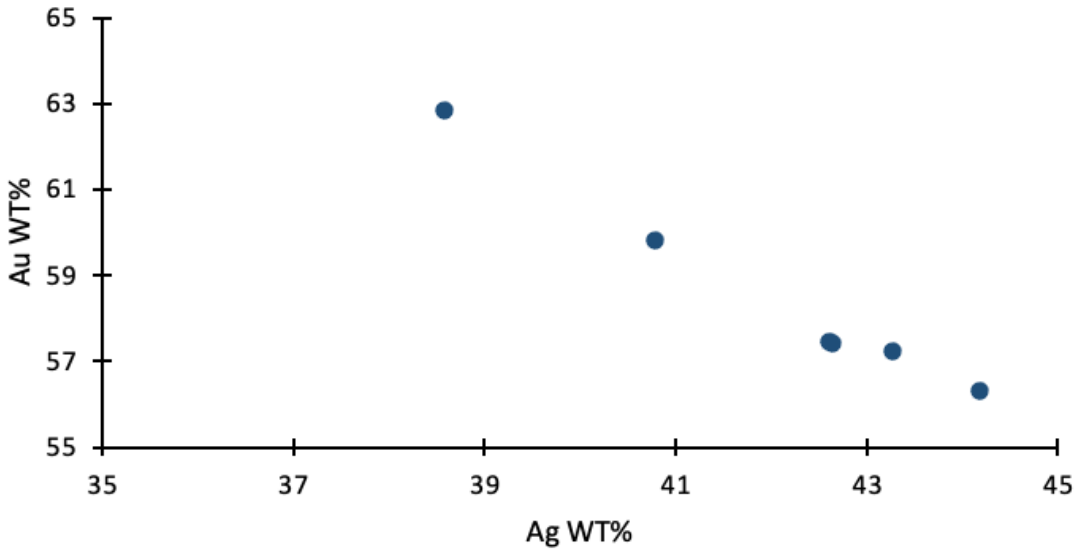

Figure 4-6: Scatter plot of electrum compositional data. Data were obtained by EMPA on sample J20-33-2 (n=6). Compositional data are listed in Table 4-2.

Table 4-2: Compositional data of electrum as determined by EMPA.

Sample	**J20-33-2**					
Spot	**#1**	**#2**	**#3**	**#4**	**#5**	**#6**
wt. %						
Ag	40.78	38.59	42.64	44.17	42.61	43.28
Au	59.84	62.86	57.40	56.31	57.44	57.24
Total	100.62	101.45	100.04	100.48	100.05	100.52
at. %						
Ag	55.45	52.85	57.56	58.89	57.53	57.99
Au	44.55	47.15	42.44	41.11	42.47	42.01
Total	100.00	100.00	100.00	100.00	100.00	100.00

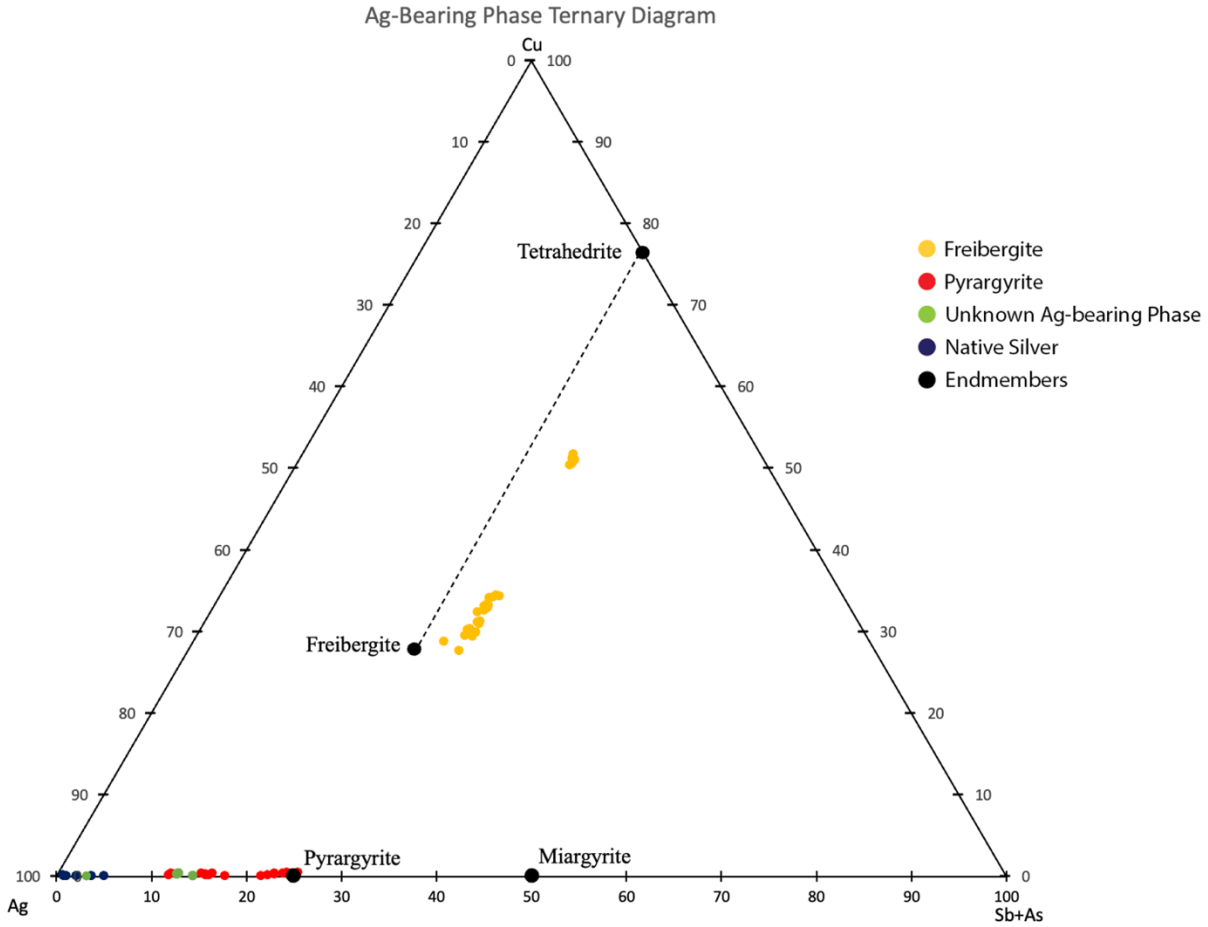

Figure 4-7: Ternary diagram displaying the compositional ranges for Ag-bearing phases. Endmembers modified from Voudouris et al. (2011).

Table 4-3: Compositional data of unidentified Ag-bearing phase as determined by EMPA.

Sample	**TV21-63-28.8**			
Spot	**#1**	**#2**	**#3**	**#4**
wt. %				
Ag	79.26	83.71	83.82	90.25
Cu	<dl	0.15	0.12	<dl
Fe	0.01	<dl	<dl	0.11
Pb	<dl	<dl	<dl	0.01
S	3.56	1.80	1.81	3.40
Sb	14.97	13.89	13.65	3.40
Zn	0.02	0.04	<dl	<dl
Total	97.82	99.59	99.40	97.17
at.%				
Ag	75.80	81.76	82.00	86.01
Cu	<dl	0.25	0.19	<dl
Fe	0.03	<dl	<dl	0.20
Pb	<dl	<dl	<dl	0.01
S	11.46	5.91	5.97	10.91
Sb	12.68	12.02	11.83	2.87
Zn	0.03	0.06	<dl	<dl
Total	100.00	100.00	100.00	100.00

Table 4-4: Representative compositional data of boulangerite as determined by EMPA.

Sample	**TV21-63-31.28**							
Spot	**#1**	**#2**	**#3**	**#4**	**#5**	**#6**	**#7**	**#8**
wt. %								
Pb	54.78	53.84	54.18	53.81	53.59	53.40	52.92	53.25
Sb	26.55	26.35	26.25	26.50	26.35	26.40	25.83	25.99
Ag	<dl	<dl	<dl	0.28	0.16	<dl	<dl	<dl
Cu	<dl	<dl	0.00	<dl	<dl	<dl	<dl	<dl
Fe	0.01	<dl	0.05	<dl	0.15	<dl	<dl	0.01
Zn	<dl	<dl	0.15	<dl	<dl	<dl	<dl	<dl
As	0.02	0.05	<dl	<dl	<dl	0.07	0.09	0.13
S	18.55	18.42	18.10	18.31	18.50	18.46	18.24	18.36
Total	99.90	98.65	98.74	98.90	98.74	98.34	97.08	97.74
apfu								
Pb	4.983	4.944	5.005	4.942	4.899	4.903	4.922	4.919
Sb	4.110	4.117	4.126	4.142	4.098	4.125	4.089	4.085
Ag	<dl	<dl	<dl	0.049	0.028	<dl	<dl	<dl
Cu	<dl	<dl	0.001	<dl	<dl	<dl	<dl	<dl
Fe	0.002		0.016	<dl	0.051	<dl	<dl	0.003
Zn	<dl	<dl	0.045	<dl	<dl	<dl	<dl	<dl
As	0.004	0.012	<dl	<dl	<dl	0.019	0.023	0.034
S	10.901	10.927	10.806	10.866	10.925	10.953	10.965	10.959
Total	20.000	20.000	20.000	20.000	20.000	20.000	20.000	20.000

4.4 Zoning and Composition of Pyrite

Backscatter electron imaging shows that many of the pyrite grains are characterized by compositional zoning, which is expressed by variations in contrast and brightness (Fig. 4-8). Combined with EDS analyses, the BSE imaging revealed that dark gray zones are characterized by low As contents whereas bright zones show distinctly high As concentrations. Compositional zoning is present in framboidal pyrite (Fig. 4-8A) as well as the subhedral to euhedral pyrite (Fig. 4-8B, C, E). Thick and more irregularly shaped bands (Fig. 4-8D) as well as angularly shaped zones occur (Fig. 4-8F).

However, the As growth zones are not present in all pyrite grains, indicating that different generations of pyrite occur. The pyrite without the As growth zones cannot be easily distinguished in reflected light from the pyrite that shows compositional zoning in BSE. Porphyroblasts of pyrite containing As and porphyroblasts containing no As are also present in the samples. The only major difference between both types of pyrite is that electrum inclusions are only present in pyrite with As-rich zones.

The composition of pyrite was determined using LA-ICP-MS point analyses. Analyzed elements included As and Au, as well as Ag, Cu, Hg, Sb, and Zn. Most analytical spots were targeted to determine the composition of the zones identifiable in BSE. Figure 4-9 shows the variations in Au content displayed on the BSE images. The corresponding data are listed in Table 4-5. The Au concentrations are highly variable.

Scatter plots showing the As content of pyrite plotted against the Au, Ag, Zn, Hg, Cu, and Sb concentrations are shown in Figure 4-10. The scatter plots do not reveal clear trends except for a weak correlation between As and Au, which is in agreement with the observed overlap between increased Au contents in pyrite and the occurrence of As-rich growth zones.

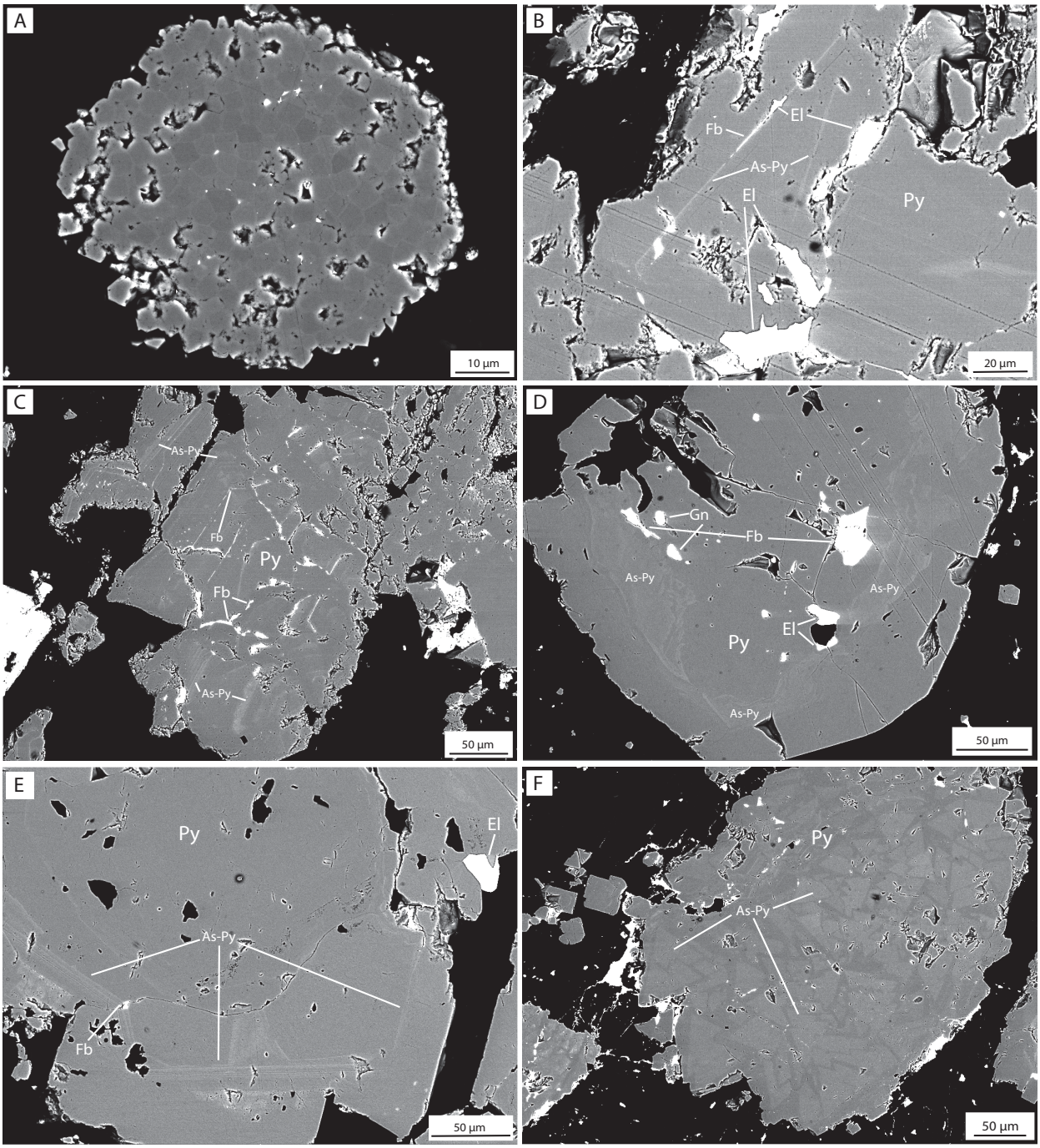

Figure 4-8: Compositional zoning in pyrite as revealed by BSE imaging. (A) Framboidal pyrite. Sample TV21-56-3. (B) Zoning in pyrite with inclusions of electrum and freibergite. Sample TV21-52-1. (C) Zoning in pyrite with inclusions of freibergite. Sample TV21-52-1. (D) Zoning in pyrite with inclusions of electrum, freibergite, and galena. Sample TV21-52-1. (E) Pyrite showing zoning with inclusions of electrum. Sample TV21-49-1. (F) Pyrite with zoning. Sample J20-33-1. Abbreviations: As-Py=As-rich pyrite, El=electrum, Fb=freibergite, Gn=galena, and Py=pyrite,

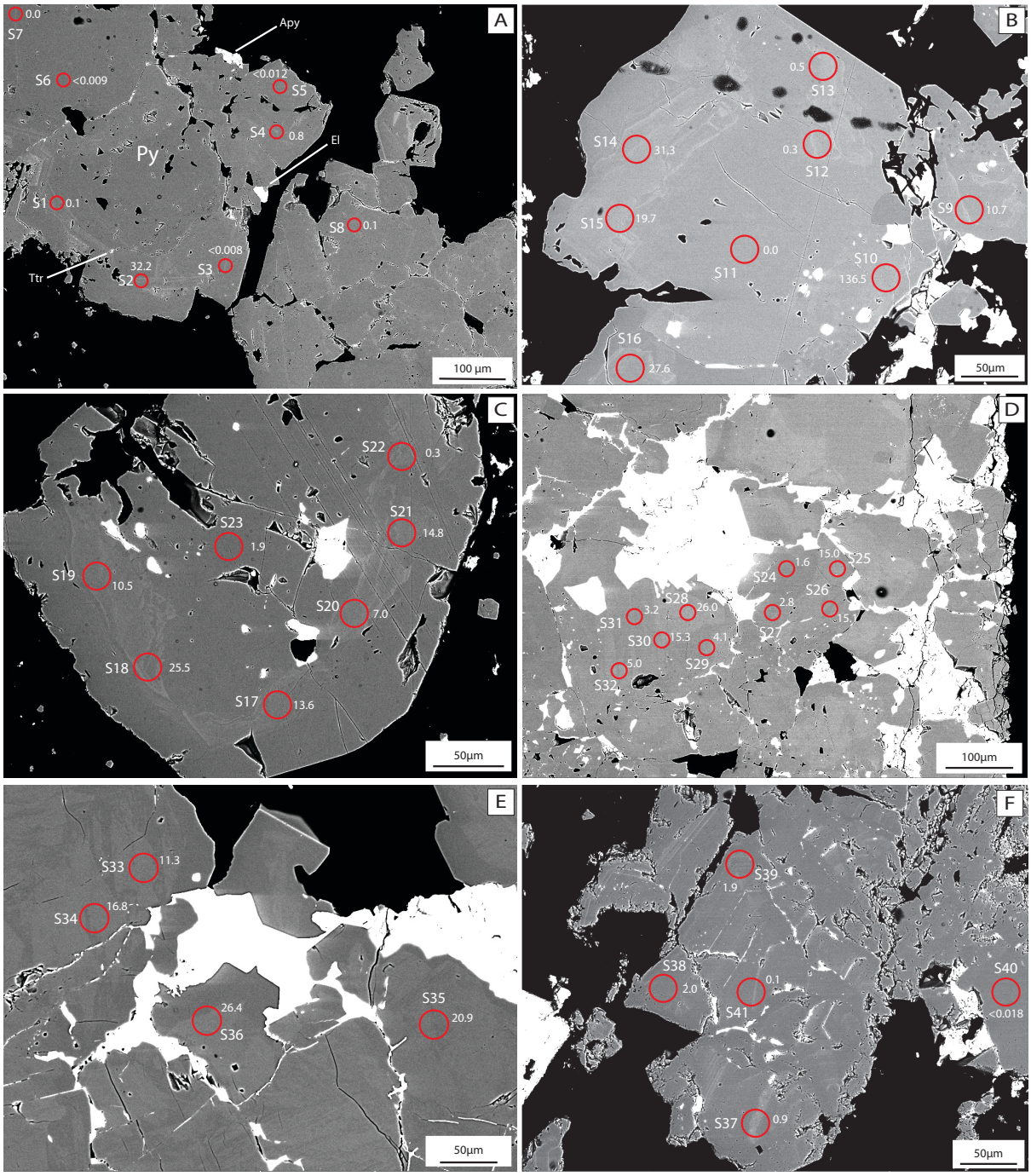

Figure 4-9: Backscattered electron images of pyrite from the TV deposit showing the locations of LA-ICP-MS spot analyses. Spot numbers and Au concentrations in ppm are shown. (A) Sample TV21-49-1. (B) Sample TV21-52-1. (C) Sample TV21-52-1. (D) Sample TV21-53-1. (E) Sample TV21-53-1. (F) Sample TV21-52-1. Abbreviation: Py=pyrite.

Table 4-5: Representative LA-ICP-MS analyses of pyrite from the TV deposit. Location of analytical spots are shown in Figure 4-9.

Spot	Au	As	Ag	Cu	Hg	Zn	Sb
S1	0.1	835	5.5	36	1	2	65
S2	32.2	1464	44.0	71	6	5	245
S3	<0.01	1036	<0.04	<0.2	1	2	34
S4	0.8	4864	2.4	26	<0.3	2	12
S5	<0.01	851	<0.07	<0.1	<0.4	2	<0.1
S6	<0.01	1888	<0.05	15	<0.3	2	11
S7	0.0	1821	0.4	0	<0.3	2	89
S8	0.1	459	1.3	2	<0.3	2	13
S9	10.7	9222	85.2	145	<0.1	2	5
S10	137	4819	963	148	1	6	25
S11	0.0	2137	0.1	1	<0.2	2	0
S12	0.3	2418	0.4	3	<0.2	2	0
S13	0.5	4767	467	19	<0.2	2	4
S14	31.3	11263	3.1	76	<0.2	1	3
S15	19.7	12365	5.0	72	<0.2	1	9
S16	27.6	19037	1.2	104	<0.2	2	1
S17	13.6	9355	5.6	69	<0.1	2	8
S18	25.5	12959	4.8	98	<0.1	2	4
S19	10.5	6104	6.7	59	<0.1	2	9
S20	7.0	8271	4.2	31	2	2	3
S21	14.8	11069	2694	1820	10	10	3201
S22	0.3	3137	12.7	9	<0.1	2	1
S23	1.9	1034	1654	31	0	2	170
S24	1.6	1590	389	135	0	12	29
S25	15.0	18141	335	114	<0.2	2	1
S26	15.1	17978	0.7	91	<0.2	2	0
S27	2.8	16423	6302	19123	12	1151	18368
S28	26.0	18786	6.2	225	<0.2	1	3
S29	4.1	3863	458	61	<2.0	2	2
S30	15.3	13330	0.4	46	<1.0	2	0
S31	3.2	5054	14.2	14	27	22696	42
S32	5.0	10830	6921	195	<0.6	3	2
S33	11.3	16333	13.5	109	<0.6	19	26

Table 4-5 (continued)

Spot	Au	As	Ag	Cu	Hg	Zn	Sb
S34	16.8	21411	189.3	447	<0.5	38	481
S35	20.9	19096	13.2	95	3	1	1
S36	26.4	23509	4.3	143	<0.4	2	3
S37	0.9	3171	11674	6926	77	18145	11291
S38	2.0	3022	360	30	54	22	597
S39	1.9	5636	2072	1095	136	202	2282
S40	<0.02	3825	0.4	0	<0.2	2	1
S41	0.1	1090	280	7	16	28246	338

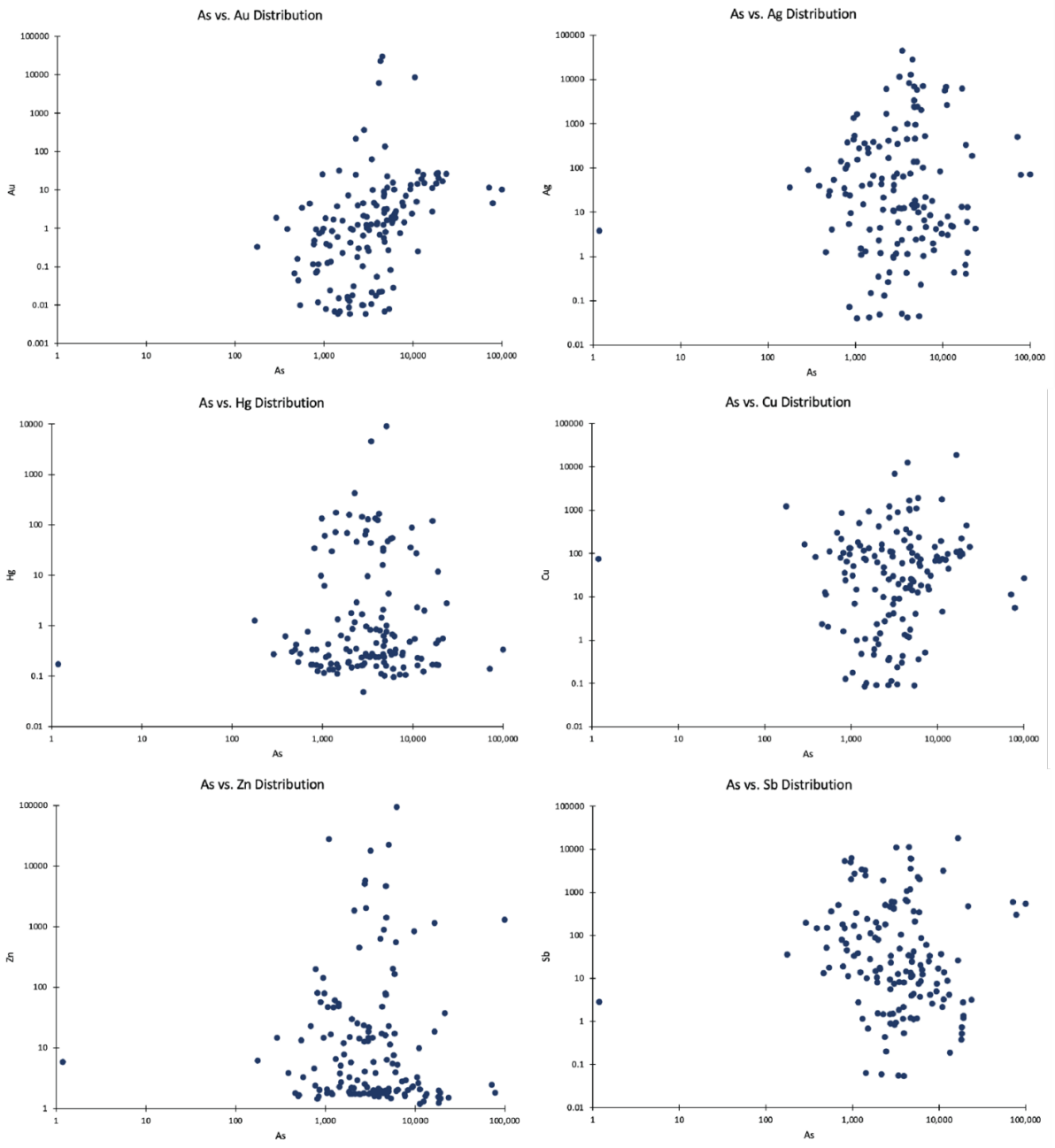

Figure 4-10: Scatter plots showing As plotted against Au, Ag, Hg, Cu, Zn, and Sb. Based on LA-ICP-MS data.

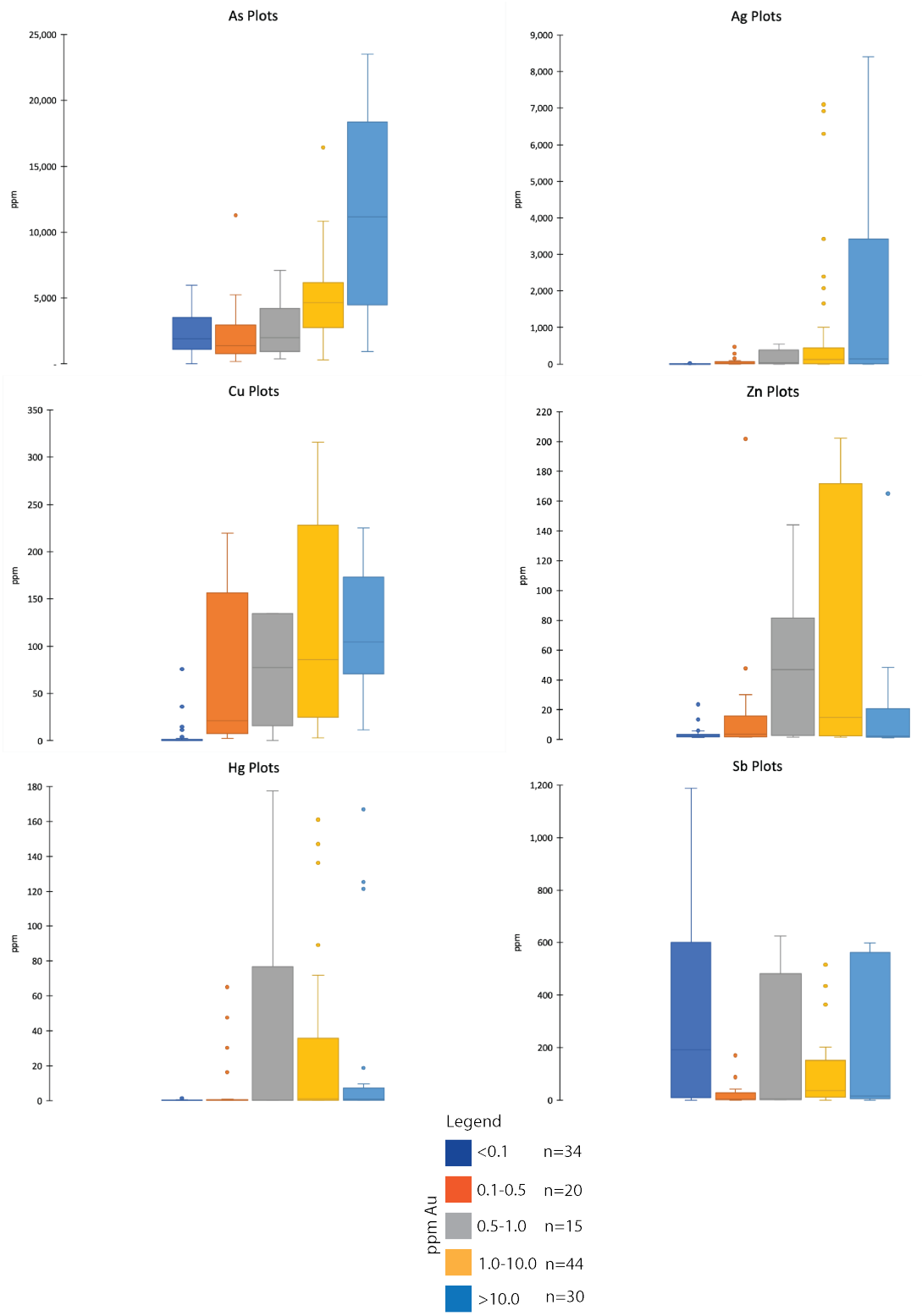

Figure 4-11: Box-and-whisker-plots showing the frequency distribution of As, Ag, Cu, Zn, Hg, and Sb assay data for different Au concentrations. Outliers falling outside the concentration ranges shown were omitted for clarity. Based on LA-ICP-MS data.

A series of box-and-whisker-plots were created to better analyze the LA-ICP-MS data. One plot shows the trace element data binned according to the Au concentrations of the analytical spots (Fig. 4-11). A relationship between Au and As concentrations can be observed at elevated Au concentrations (Fig. 4-11). At Au concentrations below 1.0 ppm, no significant differences in As can be observed. However, the As contents significantly increase at 1.0 to 10.0 ppm Au and are highest at >10.0 ppm Au. The plots suggest that As can be used as an effective pathfinder element for Au at the TV and Jeff deposits. The Ag plot shows a similar pattern. The highest Ag concentrations occur in samples with the highest Au contents.

Similar box-and-whisker plots were constructed to analyze the trace element data according to their Ag concentrations (Fig. 4-12). The plots show that the highest Ag contents correlate with elevated Sb concentrations, but also coincide with high Au, Cu, Hg, and Zn. The plots suggest a geochemical association between Ag and Sb at TV and Jeff, which is in agreement with the observed ore mineralogy. No direct relationship could be identified between Ag and As.

A box-and-whisker plot with for Sb assay data collected by Eskay Mining during the 2022 campaign at TV and Jeff was constructed using the binning for the different Ag concentrations (Fig. 4-13). The plot shows a positively linear trend, supporting the fact of an elemental association between Ag and Sb. The plot also indicates that Sb can be used as a pathfinder element for precious metal enrichment.

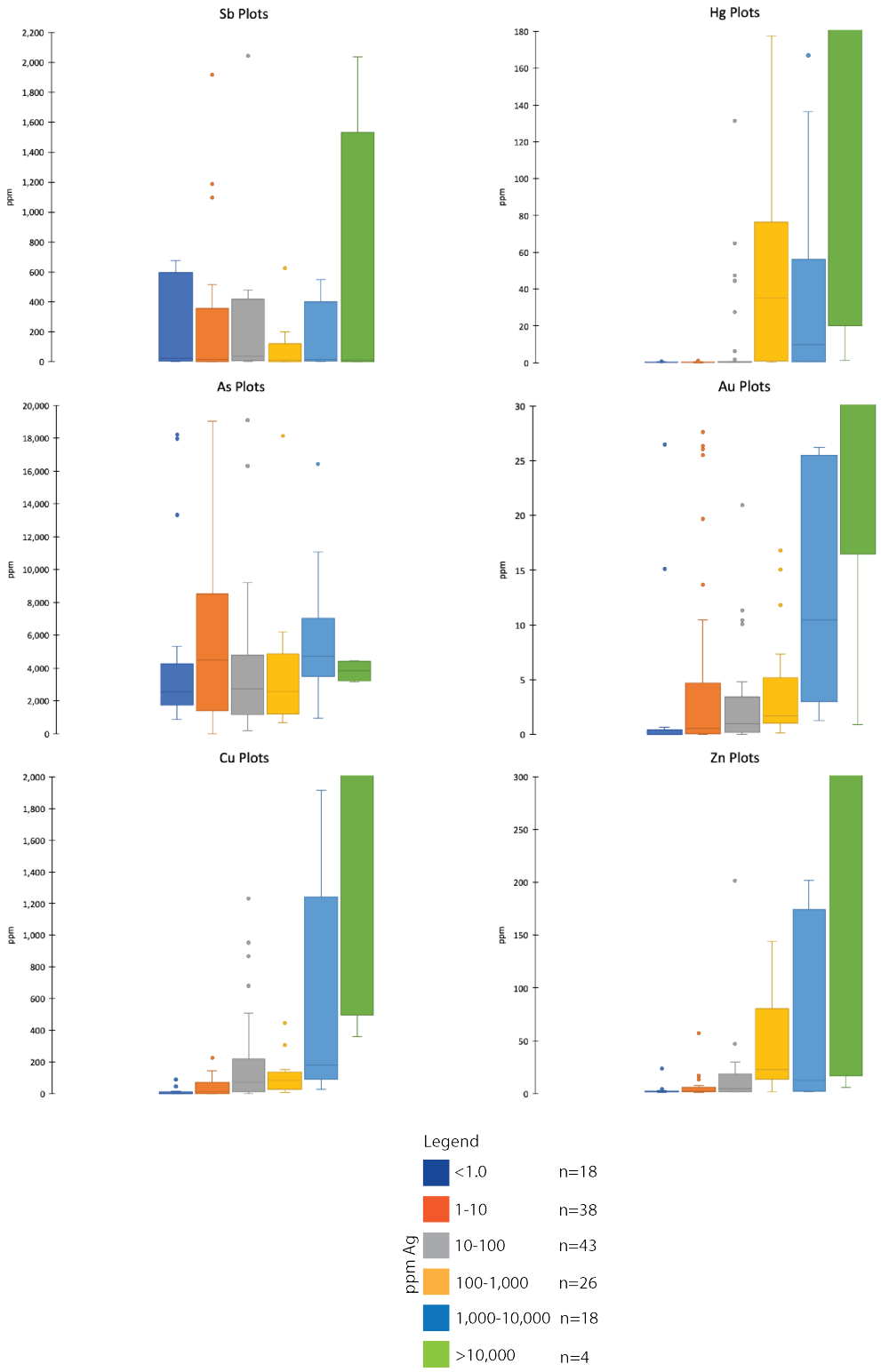

Figure 4-12: Box-and-whisker-plots showing the frequency distribution of As, Au, Cu, Zn, and Hg assay data for different Ag concentrations. Outliers falling outside the concentration ranges shown were omitted for clarity. Based on LA-ICP-MS data.

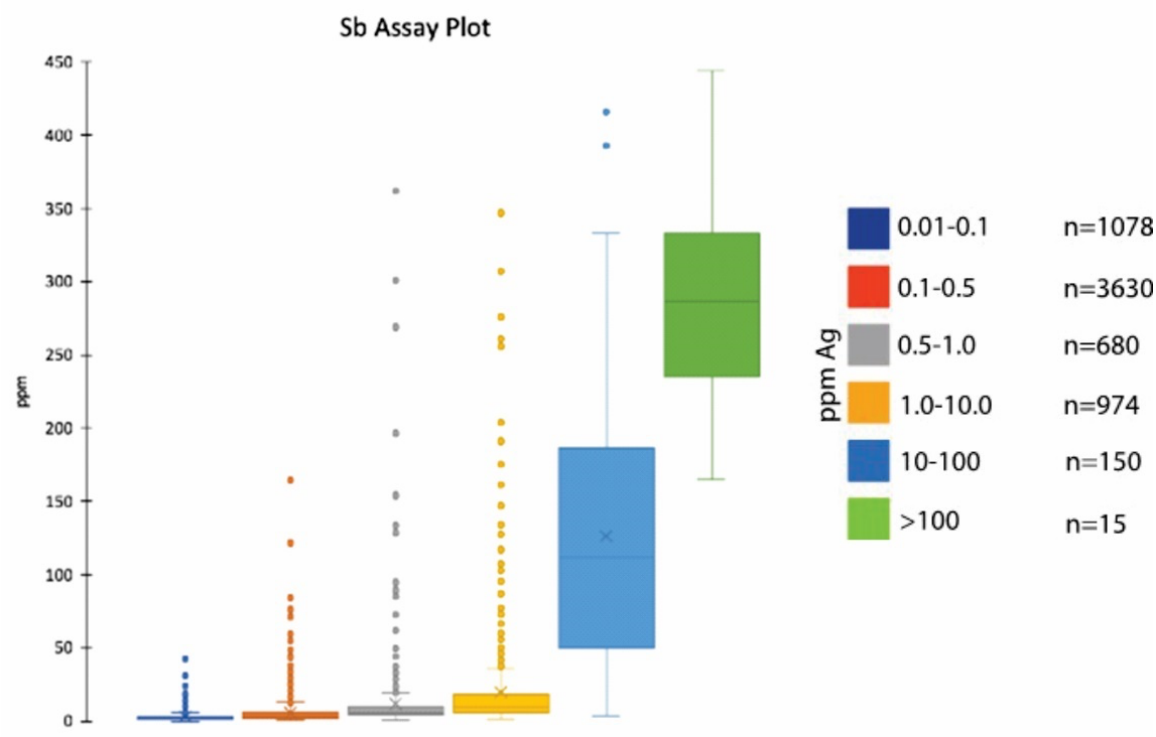

Figure 4-13: Box-and-whisker-plots showing the frequency distribution of Sb assay data binned for different Ag concentrations. Based on assay data provided by Eskay Mining Corp.

CHAPTER 5
DISCUSSION

The primary purpose of this study has been to determine the ore mineralogy of the TV-Jeff VMS deposits and the mineralogical sequestration of precious metals. The study was motivated by the discovery of the TV-Jeff deposits in the Iskut River area in proximity to the world-famous Eskay Creek deposit. Like Eskay Creek, core assays show that TV-Jeff is also characterized by precious metal grades unusual for VMS deposits. This study chapter discusses the research findings and derives recommendations for further exploration in the Iskut River area.

5.1 Mineral Paragenesis

A paragenetic model of sulfides, sulfosalts, and alloys is presented in Figure 5-1. There are three distinct stages of mineralization, namely a pre-ore stage, an ore stage, and deformation/metamorphic stage. Framboidal pyrite represents the beginning of sulfide mineralization (Figs. 4-1A and 4-8A). The framboidal pyrite forms from the formation and aggregation of greigite (Fe_3S_4) microcrystals, followed by subsequent replacement by pyrite (Wilkin and Barnes, 1997). Greigite forms at low temperatures suggesting the botryoidal pyrite formed during the waxing stages of the hydrothermal system.

Formation of subhedral to euhedral pyrite occurred in both the pre-ore and ore stages and occur as both As-poor and As-rich. The As-rich pyrite is commonly seen with precious and base metals, whereas the As-poor pyrite does not show the same mineral association. The As-rich pyrite commonly displays compositional zoning, which is growth zoning in many cases. The growth zones are primary but have also been affected by deformation and recrystallization (Fig. 4-8D, F). These growth zones are commonly associated with electrum, freibergite, and galena, implying a metal association of As-Au-Ag-Cu-Pb-Sb. The As-rich pyrite marks the beginning of precious-metal deposition at the TV and Jeff deposits.

Galena has a strong association with electrum and many Ag-bearing minerals, including native Ag. Native Ag occurs as bladed aggregates and in large masses greater than 500 μm with

a characteristic black rim under SEM (Fig. 4-5A, B). The latter shows native Ag deposition before the other Ag-bearing minerals pyrargyrite and freibergite, as well as galena (Fig. 4-5A). Pyrargyrite crosscuts and rims pyrite and sphalerite (Fig. 4-5D), suggesting pyrargyrite and other Ag-bearing minerals formed after pyrite and sphalerite during the ore stage. The same is true for boulangerite (Fig. 4-5C) and other lead sulfosalts.

Sphalerite from TV and Jeff frequently shows chalcopyrite disease, observed by blebs of chalcopyrite within sphalerite (Fig. 4-1D). According to Govindarao et al. (2018), chalcopyrite disease is indicative of Fe-rich sphalerite and can be caused by sulfide partial melting, which would suggest that the chalcopyrite disease formed under amphibolite grade metamorphism. However, amphibolite conditions required for sulfide partial melting to occur were not achieved at TV and Jeff, which underwent greenschist metamorphism. The chalcopyrite disease present in TV and Jeff is, therefore, more likely a primary texture. According to Nagase and Kojima (1997) chalcopyrite disease in the hydrothermal environment can occur from either replacement or coprecipitation. Replacement in the form of either fine lamellae or ellipsoidal to lens-like textures occurs in Fe-rich sphalerite, and coprecipitation in the form of triangular to irregular blebs occurs in Fe-poor sphalerite (Nagase and Kojima, 1997). TV and Jeff contain Fe-bearing sphalerite, which supports the hypothesis that the chalcopyrite disease formed by replacement. The fine lamellae and subsequent lens-like growth from these lamellae shown in Figure 4-1D also supports this. According to Barton and Bethke (1987), chalcopyrite replacement in sea-floor massive sulfide deposits occurs at temperatures of 200–400°C without a later and higher temperature fluid overprint. The temperature range for chalcopyrite replacement suggests that low temperatures around 200°C could have persisted to the end of precious-metal deposition at TV and Jeff, indicated by chalcopyrite's paragenetic placement.

The hydrothermal fluids forming TV and Jeff were initially low temperature, indicated by the presence of framboidal pyrite. The compositional zoning of As in pyrite marked the next stage of the fluid evolution, which was the introduction of precious and base metals. The pyrite zoning records a metal association of As-Au-Ag-Cu-Pb-Sb-Hg. Those elements can be used as pathfinder elements for the precious metals. During the subsequent fluid evolution, the hydrothermal fluids reached temperatures of at least 200°C to allow for the formation of

chalcopyrite disease (Barton and Bethke, 1987), with most chalcopyrite likely forming at 250–350°C (Hannington et al., 1995). The precipitation of minerals in the ore-stage at or around the same time is most likely due to quenching of the hydrothermal fluids by seawater (Hannington et al., 1995).

The sulfide and sulfosalt mineralogy is similar at the TV and Jeff deposits. Both contain abundant pyrite. Sphalerite, galena, pyrrhotite, and chalcopyrite are present in both deposits albeit in relatively small amounts. The birds-eye pyrite and marcasite replacing pyrrhotite were only observed at TV. Arsenopyrite is also more abundant at the TV deposit. Electrum is the main Au-bearing phase and is texturally the same in both deposits. Electrum grains are located along grain boundaries, as well as in fractures and veinlets of pyrite. Electrum is also commonly associated with galena in both deposits. The gold grade in the samples from this study is highest in Jeff with drillhole J20-33 containing 81.2 ppm Au, while the highest Au grade from the TV samples is from TV21-53 at 24.6 ppm Au. Both deposits contain abundant Ag minerals. By far, the highest Ag assay grade from the samples studied is from drillhole TV21-63 from 28-29m at 2,640 ppm Ag. Both deposits contain freibergite, pyrargyrite, and acanthite. However, native Ag was only observed in TV samples. Diaphorite and the unknown Ag-bearing phase are also only present at TV. Boulangerite is present in both deposits. The similar ore mineralogy from both deposits suggests the hydrothermal fluids were very similar, possibly suggesting that both deposits formed as part of a larger hydrothermal system. The presence of more Ag-sulfosalts in samples from TV could be the result of sample bias or indicate more than one source of hydrothermal fluids. More samples need to be analyzed to accurately determine which is correct.

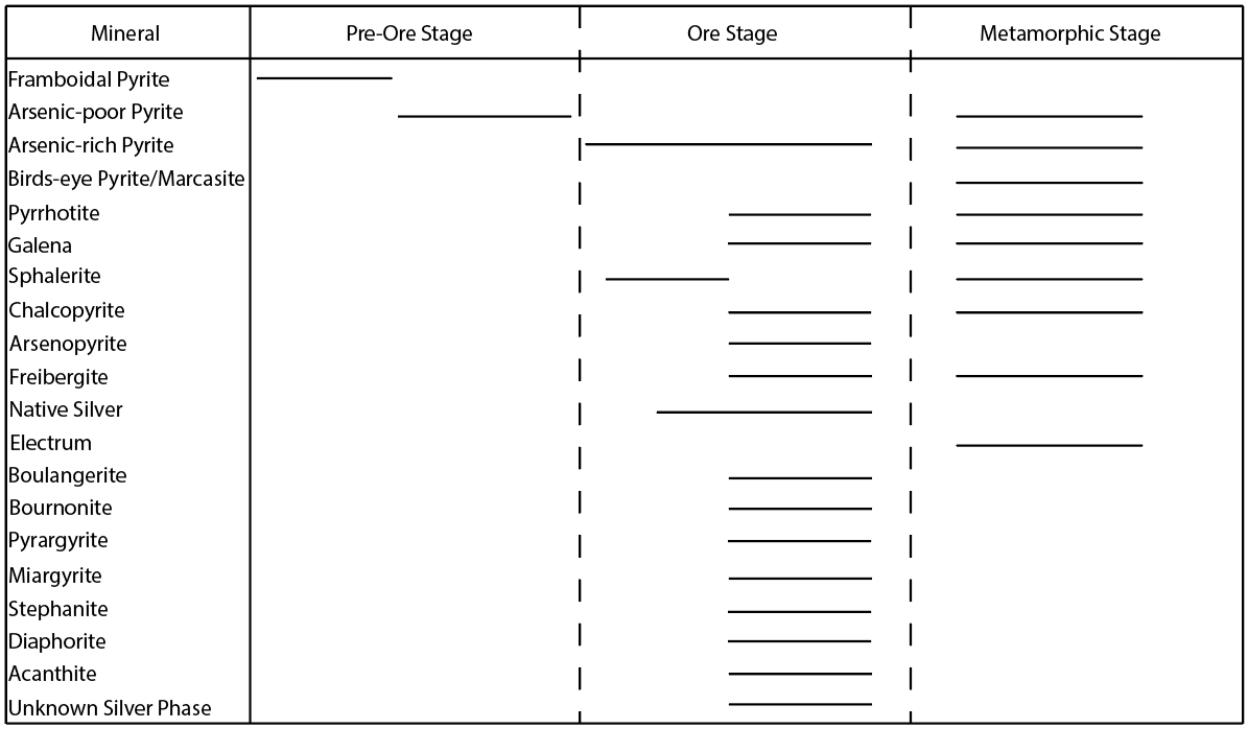

Figure 5-1: Paragenetic diagram for ore minerals at the TV and Jeff deposits.

5.2 Mineralogical Sequestration of Gold

This study establishes that the Au observed is in pyrite, which includes both electrum inclusions in arsenian pyrite and structurally bound Au. The structurally bound gold is invisible and would require processing of the pyrite using an autoclave or similar techniques. Similar invisible Au has been described from other VMS deposits (Healy and Petruk, 1990; Huston et al., 1992).

Electrum was the only Au-bearing phase identified using optical microscopy. In many cases electrum is apparently texturally late and occurs along fractures or in small veins, which may suggest that Au is remobilized at the small scale. It is envisaged here that much of the electrum was liberated from the pyrite during metamorphism and deformation, as initially suggested by Huston et al. (1992). The textural observations argue against the free electrum grains being primary precipitates from the mineralizing fluids.

Metamorphic recrystallization of pyrite containing invisible Au has been shown to be a significant mechanism for Au liberation in VMS deposits (Huston et al. 1992; Wagner et al., 2007). Au in VMS deposits that have been overprinted at upper greenschist to amphibolite grade metamorphism is typically significantly redistributed (Larocque and Hodgson, 1993; Marshall et al., 2000; Wagner et al., 2007). Redistributed Au exists as free electrum, making the Au extraction process easier (Wagner et al., 2007). Increased recrystallization results in the reduction of invisible Au and an increase in free electrum (Wagner et al., 2007). The textural setting of Au is influenced by microscale processes. The brittle deformation of pyrite plays a central role in creating fractures and pathways for Au redeposition in the metamorphic environment (Larocque and Hodgson, 1993) explaining why electrum at TV and Jeff apparently always crosscuts more brittle phases such as pyrite on the microscale.

5.3 Recrystallization and Remobilization

Pyrite at the TV and Jeff deposits shows extensive evidence for recrystallization (Figs. 4-1 and 4-2). In many cases primary pyrite, both As-poor and As-rich, has recrystallized to porphyroblasts that are euhedral to subhedral in shape (Figs. 4-1 and 4-2). The pyrite porphyroblasts are located in a matrix of base metal sulfides that experienced ductile deformation. Many of the relationships between the sulfide minerals are not primary despite the fact that TV and Jeff were only overprinted at greenschist facies conditions (Lindsay et al., 2021), suggesting deformation played a major role in redistribution.

Marshall and Gilligan (1987) showed that metamorphic remobilization in massive sulfides occurs by mechanical, chemical, or mixed processes. Verified experimentally, it was demonstrated that brittle and ductile deformation result in mechanical remobilization (Marshall and Gilligan, 1987). This occurs at the micro- and macro-scale, however; it is much more common at the microscale (Marshall and Gilligan, 1987). Macroscale mechanical remobilization is more likely to occur at conditions of 350–500°C, which corresponds to greenschist to amphibolite metamorphism (Marshall and Gilligan, 1987). Ductile deformation at TV and Jeff is observed only with the sulfides (Fig. 4-2), suggesting it occurs on the micro scale.

Base metal sulfides remobilize through mechanical processes, but chemical processes can also play a role (Marshall and Gilligan, 1987). The mechanical and chemical processes are commonly mixed during remobilization, especially during fluid-present metamorphism (Marshall and Gilligan, 1987). Ductile remobilization has the capability to form ore shoots and subsequently upgrade (Marshall and Gilligan, 1993). Ductile deformation was an important process in the mechanical remobilization of base metals at the Montauban Zn-Pb-Au-Ag deposit in Canada (Tomkins, 2007). However, Au and Ag mineralization at Montauban was most affected by a combination of prograde hydrothermal remobilization and sulfide partial melting (Tomkins, 2007). Au and Ag are soluble in hydrothermal fluids as sulfide complexes, which allows the hydrothermal remobilization of these elements to occur (Gammons and Barnes, 1989; Loucks and Mavrogenes, 1999; Tomkins, 2007). According to Tomkins (2007) prograde metamorphic hydrothermal remobilization occurs at metamorphic conditions approaching amphibolite facies, and metamorphic sulfide partial melting commences in the middle amphibolite facies.

Fluid-phase remobilization is also thought to have played a significant role in the Gressli deposit in the central Norwegian Caledonides (Vokes and Craig, 1993). Chalcopyrite and sphalerite at this deposit form a ductile matrix in fractures and grain boundaries surrounding pyrite porphyroblasts, exhibiting replacement relationships with the pyrite (Vokes and Craig, 1993). The replacement of the pyrite with the chalcopyrite and sphalerite indicates fluid phase remobilization (Vokes and Craig, 1993). The base metal sulfides in the pyrite fractures indicate that they were deposited close to or at the site of original deposition (Vokes and Craig, 1993). Sulfur isotope signatures were used by Wagner et al. (2005) to determine metamorphic sulfide remobilization in the Hällefors district in Bergslagen, Sweden. The deposits in this district show both stratabound sulfide and discordant, Ag-rich sulfide and sulfosalt veins (Wagner et al., 2005). Through their sulfur isotope signature results, Wagner et al. (2005) determined that the vein-type ore formed from metamorphic remobilization from the stratabound massive sulfides. They came to this conclusion because the $\delta^{34}S$ of the vein ore and the massive sulfide ore were very similar, indicating that the massive sulfides supplied most of the sulfur for the veins (Wagner et al., 2005). This metamorphic remobilization occurred at greenschist facies conditions of 300–400°C and 2–3 kbar (Wagner et al., 2005).

At TV and Jeff, recrystallization textures such as pyrite porphyroblasts, brittle deformation of pyrite, and ductile behavior and remobilization of base metal sulfides can be observed. Precious-metal remobilization is also observed, indicating prograde hydrothermal remobilization. These factors support the hypothesis that base and precious metal remobilization occurred through mixed processes and fluid-phase remobilization at greenschist facies conditions. However, sulfide partial melting described by Tomkins (2007) did not occur as metamorphic conditions at TV and Jeff did not reach amphibolite grade.

5.4 Comparison to Au-rich VMS Deposits

The past producing Eskay Creek VMS deposit shares some similarities with the TV and Jeff deposits, but also has some key differences. TV, Jeff, and Eskay Creek all are located within the Jurassic Hazelton Group (Lindsay et al., 2021; Roth et al., 1999). Eskay Creek is located within the Eskay anticline, which is a north plunging, north-northeast trending upright open fold (Roth et al., 1997). TV and Jeff are also in east-facing folded volcanic rocks of the Hazelton Group further to the southeast. The deposits occur at different stratigraphic positions. While the host rocks of TV and Jeff belong to the Betty Creek Formation of the lower Hazelton Group, the Eskay Creek deposit lies in the Iskut River Formation of the upper Hazelton Group (Nelson et al., 2018). According to current geochronological constraints (Nelson et al., 2018), this makes TV and Jeff deposits from the early Jurassic, approximately 193 Ma, whereas Eskay Creek is middle Jurassic with an age of 175±2 Ma (Childe, 1996). The significant age difference implies that TV-Jeff and Eskay Creek did not form in the same volcanic basin.

Gold at Eskay Creek is hosted primarily in electrum although amalgam is also present (Roth et al., 1997). The ore mineralogy includes pyrite, chalcopyrite, sphalerite, galena, tetrahedrite, freibergite, pyrargyrite, bournonite, boulangerite, arsenopyrite, stibnite, realgar, and cinnabar (Roth et al., 1997). While many of these minerals are present in TV and Jeff, the presence of stibnite, realgar, and cinnabar has not been detected in any of the samples from this study. Pyrrhotite does not appear to form part of the sulfide assemblage at Eskay Creek (Roth et al., 1997). It is not well documented whether invisible Au in arsenian pyrite was important at Eskay Creek.

The base metal content of the ores at Eskay Creek is not well constrained as the deposit was mined as an Au-Ag deposit and base metal production is not reported. Sherlock et al. (1999) reported that the deposit contained a total of 1.9 million tons of ore grading 60.2 g/t Au, 2,645 g/t Ag, 3.2 wt. %Pb, 5.2 wt. % Zn, and 0.7 wt. % Cu. This makes Eskay Creek a VMS deposit of the Au-Zn-Pb-Ag element association (Huston, 2000).

The main types of alteration at TV and Jeff are silicification, clay, carbonate, chlorite, barium-feldspar, and white mica alteration (Peterson, 2022). The style and intensity of alteration at TV and Jeff suggest that the deposits formed vent proximal, and that the hydrothermal fluids formed at low temperatures (<250°C; Peterson, 2022; Large et al., 2001). The mineralized zones at Eskay Creek are associated with a similar style of alteration. The footwall rhyolite displays a quartz-sericite-pyrite-potassium feldspar-chlorite alteration assemblage (Roth et al., 1997). Sulfides such as pyrite, sphalerite, galena, and chalcopyrite are associated with zones of intense alteration (Roth et al., 1997).

The metamorphic grade at Eskay Creek is very similar to TV and Jeff. The regional metamorphic grade at Eskay Creek is prehnite-pumpellyite to lower greenschist (Britton et al., 1990; Roth et al., 1997; T. Monecke, personal comm. 2022). However, the metamorphic grade appears to increase towards the south (Lindsay et al., 2021) and reaches greenschist to upper greenschist facies at TV and Jeff.

Aside from Eskay Creek, there are several Au-rich VMS deposits worldwide, including the Horne and LaRonde Penna deposits in the Archean Abitibi greenstone belt in Quebec, Canada, and the Boliden deposit in the Proterozoic Skellefte district of Sweden (Mercier-Langevin et al., 2011). The Au-rich Horne deposit in the Archean Abitibi greenstone belt of eastern Canada has a Au grade of 6.10 g/t and contains a total endowment of 327.6 metric tons of Au. There is a Au-Cu association as the ores contain 2.2 wt. % Cu on average (Mercier-Langevin et al., 2011). The deposit formed during the Archean at 2702–2701 Ma in a back-arc basin setting (Mercier-Langevin et al., 2011). The host rocks are mostly tholeiitic to transitional felsic volcaniclastic deposits, as well as tholeiitic pillowed mafic rocks (Mercier-Langevin et al.,

2011). The volcanic succession at Horne has been overprinted at greenschist metamorphic grade (Monecke et al., 2008, 2017). The sulfides are disseminated, massive, and in stringers, with pyrite being the most abundant sulfide (Kerr and Mason, 1990; Gibson et al., 2000; Monecke et al., 2008). Alteration includes chlorite and sericite-chlorite-quartz (Kerr and Mason, 1990; Gibson et al., 2000; Monecke et al., 2008, 2017).

The LaRonde-Penna deposit is also located in the Archean Abitibi greenstone belt of Quebec. LaRonde-Penna has a Au grade of 4.31 g/t for a total endowment of 253 metric tons. The deposit contains on average 0.3 wt. % Cu and 2.2 wt. % Zn (Mercier-Langevin et al., 2007; 2011). The deposit is hosted by 2,698 Ma volcanic rocks interpreted to have formed in a submarine back-arc basin or rift (Mercier-Langevin et al., 2007; 2011). The ores are hosted by tholeiitic to transitional mafic and intermediate rocks, as well as transitional to calc-alkaline felsic rocks (Mercier-Langevin et al., 2007; 2011). The sulfides are semi-massive to massive and in stringers, with pyrite being the most abundant sulfide (Mercier-Langevin et al., 2007; 2011). The deposit occurs in stacked lenses with Au-Cu and Au-Zn-(Pb)-Ag element associations (Mercier-Langevin et al., 2011). The metamorphic grade at LaRonde-Penna is amphibolite (Dubé et al., 2007).

The Boliden deposit, located in the Paleoproterozoic Skellefte district in Sweden, is a precious metal-rich VMS deposit with a Au grade of 15.5 g/t and a total Au endowment of 128.7 metric tons (Mercier-Langevin et al., 2011). It contains base metal concentrations of 1.5 wt. % Cu, 0.9 wt. % Zn, and 0.3 wt. % Pb (Mercier-Langevin et al., 2011). The deposit formed in the Paleoproterozoic at around 1,885–1,880 Ma in a submarine continental margin volcanic arc (Bergman Weihed et al., 1996; Mercier-Langevin et al., 2013). The host rocks are mostly transitional felsic to intermediate rocks, including dacitic to rhyolitic volcaniclastic deposits and lava domes, as well as andesitic rocks (Bergman Weihed et al., 1996; Mercier-Langevin et al., 2011). The sulfides are disseminated or massive, forming a Au-As-Cu elemental association, with arsenopyrite being the second most abundant sulfide at Boliden (Mercier-Langevin et al., 2011). The metamorphic grade in the Skellefte district is greenschist to amphibolite grade (Wagner et al., 2007).

Comparison of the different Au-rich deposits shows that there are no unifying mineralogical characteristics. Precious metal enrichment occurs in association with various elements, including the Au-Cu association at Horne, the Au-Zn-(Pb)-Ag association at LaRonde-Penna and Eskay Creek, and the Au-As-Cu association at Boliden. The TV and Jeff deposits are characterized by pyritic ores with distinctly low base metal concentrations. While TV and Jeff do host base metal sulfides, they do not have economic base metal associations like the other Au-rich VMS described above. All Au-rich deposits are hosted by felsic to intermediate volcanic wall rock, with the wall rocks of the sulfide ores being overprinted by sericite-chlorite-quartz or chlorite alteration. In some Au-rich deposits, carbonate alteration is important or may have been present prior to metamorphic reequilibration at amphibolite facies grades. The TV and Jeff deposits as well as Eskay Creek are unusual as low-temperature K-feldspar alteration is associated with the Au-rich ores, which is consistent with the inferred low (<250°C) temperature of ore formation (Schardt et al., 2001). The similarities and differences of TV and Jeff to the above-mentioned Au-rich VMS deposits indicates that there is not one model for a Au-rich VMS deposit. However, the similar wall rocks and metamorphic grades are unifying characteristics that can be used as indicators for precious-metal enrichment.

5.5 Exploration Implications

The findings of this research have some important implications to exploration for VMS deposits in the Iskut River area. As noted by Lindsay et al. (2021) and Peterson (2022), the discovery of the TV and Jeff deposits suggests that the Iskut River area represents a VMS camp and that the Eskay Creek deposit is not the only deposit within the camp. Currently available data suggests that the TV and Jeff deposits are located stratigraphically below the Eskay Creek deposit, implying the existence of more than one favorable horizon within the camp. This is comparable to other VMS camps, many of which show two or more stratigraphic positions at which VMS deposits are located (Allen et al., 2002; Monecke et al., 2017). This is significant from an exploration perspective as it opens up significant new ground for the search for VMS deposits.

The age difference between the lower and upper Hazelton groups poses significant questions as to how well understood the stratigraphic make-up of the Iskut River area really is. It

appears possible that the volcanic rocks of the lower and the upper Hazelton groups are not in depositional contact and only structurally juxtaposed. Alternatively, it would need to be considered that current geochronological constraints are not correctly interpreted. Future exploration in the Iskut River area will require improved understanding of the stratigraphic relationships.

The mineralogical investigations of this study show that TV and Jeff are unusual VMS deposits. Similar to Eskay Creek, precious-metal enrichment at these deposits is not associated with significant enrichment of base metals. This contrasts with many other Au-rich VMS deposits where Au-enrichment occurs in Au-Cu association (e.g., Horne deposit in Quebec) or in Au-Zn-Pb-Ag association (e.g., LaRonde-Penna in Quebec). Precious metal enrichment at TV and Jeff is associated with low-temperature pyritic ores. A proportion of the Au contained occurs as invisible Au in As-bearing pyrite. Some, if not all, electrum appears to have formed from recrystallization of pyrite during metamorphism and deformation and the liberation of the Au from the pyrite crystal structure. Although the presence of Au in As-bearing pyrite is not unusual in VMS deposits (Huston et al., 1992; Huston et al., 2000; Mercier-Langevin et al., 2011), the occurrence of pyritic deposits with high precious metal concentrations and low base metal contents is not commonly described in the literature, making these deposits potentially new exploration targets in other VMS camps where previous exploration may have focused on polymetallic deposits.

The study confirms that As is likely the best pathfinder element for Au at TV and Jeff and similar deposits. Elevated Sb concentrations appear to be associated with high Ag concentrations. As hand-held XRF can be used to measure Ag, As, and Sb in whole-rock samples and drill core, the use of this instrumentation is undoubtedly warranted to conduct targeting while assays are obtained by conventional laboratory analyses.

CHAPTER 6
CONCLUSIONS

This chapter summarizes the key findings of this study and provides suggestions for further work at the TV and Jeff deposits. The findings of this research have implications to the understanding of Au-rich VMS deposits and the development of exploration strategies for pyritic deposits having elevated precious metal grades.

6.1 Research Findings

1. TV and Jeff are important new discoveries of Au-rich VMS deposits in the Iskut River area of northern British Columbia. The deposits occur in the Jurassic Hazelton Group, which is also host to the world-class Eskay Creek deposit. However, TV and Jeff appear to be localized lower in stratigraphy suggesting the existence of more than one favorable horizon within the area. TV and Jeff are dominantly pyritic deposits that have elevated precious metal grades.

2. Microscopic investigations on the pyritic ores show that primary depositional textures are present at TV and Jeff. However, the deformation and greenschist metamorphic overprint have resulted in the recrystallization of the sulfide assemblages and widespread textural modification. Recrystallization at greenschist metamorphic grades is underreported in the literature.

3. This study shows that metamorphic recrystallization is an important process resulting in the conversion of invisible Au to free electrum. It is shown that a significant proportion of the Au at TV and Jeff is contained in As-rich pyrite. During recrystallization, Au originally contained in the crystal structure of pyrite forms small electrum inclusions in As-rich growth zones or is mobilized into fractures and veins. Recrystallization has also affected the base metal sulfides, which commonly form a ductile matrix surrounding pyrite porphyroblasts and pyrite grains that have been affected by brittle deformation.

4. TV and Jeff are pyritic Au-rich VMS deposits. They share a number of characteristics with other VMS deposits that show high Au grades, but the metal association differs significantly. In contrast to the nearby Eskay Creek deposit, TV and Jeff are not characterized by a Zn-Pb-Ag element association, or zones of base metal enrichment have not yet been identified. Precious metal enrichment at TV and Jeff is interpreted to have occurred at distinctly low-temperatures of ~200°C or below.

6.2 Recommendations for Future Work

Based on the research conducted, a number of recommendations for future work are made:

1. Further systematic microanalytical work should focus on testing whether As-rich and As-poor pyrite can be distinguished at all using reflected light microscopy and to establish potential paragenetic relationships between both pyrite generations. Identifying the reason(s) why some pyrite is barren while texturally similar pyrite is mineralized has important implications to future exploration as the use of pathfinder elements such as As is currently the only tool available to explorationists to distinguish both pyrite types in the field.

2. It is proposed here to conduct additional microanalytical work including electron microprobe analysis on more samples to allow more statistically relevant conclusions and to test for potential compositional gradients across the two deposits. Additional microanalytical work is recommended to conclusively identify the nature of the unknown silver-bearing phase.

3. Assay data from Eskay Mining should be used to identify potential gradients in base metal grades that could be used to reconstruct temperature gradients across the deposits and to identify hydrothermal upflow zones. When combined with the results of microanalytical work as conducted here, this may provide new important insights into the anatomy of the hydrothermal system at TV and Jeff.

4. Sulfur isotope signatures should be tested in the future to better determine the source of the hydrothermal fluids and to test for a potential magmatic component. Sulfur isotopes could also be used to assist in the reconstruction of metamorphic sulfide remobilization.

5. The role of deformation processes coupled with metamorphism should be examined to more accurately determine the mechanisms for redistribution of precious metals.

6. The observed paragenesis should be refined further and used to interpret hydrothermal processes that led to precious-metal deposition.

REFERENCES

Alldrick, D.J., Stewart, M.L., Nelson, J.L., and Simpson, K.A., 2004, Tracking the Eskay Rift through northern British Columbia - Geology and mineral occurrences of the Upper Iskut River area (Telegraph Creek NTS 104G/1, 2, 7, 8, 9, 10): British Columbia Ministry of Energy and Mines, Geological Fieldwork 2003, Paper 2004-1, 18 p.

Alldrick, D.J., Nelson, J.L., and Barresi, T., 2005, Geology and mineral occurrences of the upper Iskut River area: Tracking the Eskay Rift through northern British Columbia (Telegraph Creek NTS 104G/1, 2; Iskut River NTS 104B/9, 10, 15, 16): British Columbia Ministry of Energy, Mines and Petroleum Resources, Geological Fieldwork 2004, Paper 2005-1, 30 p.

Allen, R.L., Weihed, P., Blundell, D., Crawford, T., Davidson, G., Galley, A., Gibson, H., Hannington, M., Herrington, R., Herzig, P., Large, R., Lentz, D., Maslennikov, V., McCutcheon, S., Peter, J., and Tornos, F., 2002, Global comparisons of volcanic-associated massive sulphide districts, in: Blundell, D.J., Neubauer, F., and Von Quadt, A. (eds.), The timing and location of major ore deposits in an evolving orogen: Geological Society, London, Special Publications, v. 204, p. 13–37.

Anderson, R.G., 1989, A stratigraphic, plutonic, and structural framework for the Iskut River map area, northwestern British Columbia: Geological Survey of Canada Paper 89-1E, p. 145–154.

Barrett, T.J., and Sherlock, R.L., 1996, Geology, lithogeochemistry, and volcanic setting of the Eskay Creek Au-Ag-Cu-Zn deposit, northwestern British Columbia: Exploration Mining Geology, v. 5, p. 339–368.

Barton, P.B., and Bethke, P.M., 1987, Chalcopyrite disease in sphalerite: Pathology and epidemiology: American Mineralogist, v. 72, p. 451–467.

Bartsch, R.D., 1993, A rhyolite flow dome in the Upper Hazelton Group, Eskay Creek area (104B/9, 10): British Columbia Ministry of Energy, Mines and Petroleum Resources Paper 1993-1, Geological Fieldwork 1992, p. 331–334.

Bergman Weihed, J., Bergström, U., Billström, K., and Weihed, P., 1996, Geology, tectonic setting, and origin of the Paleoproterozoic Boliden Au-Cu-As deposit, Skellefte district, northern Sweden: Economic Geology, v. 91, p. 1073–1097.

Britton, J.M., Webster, C.L., and Alldrick, D.J., 1989, Unuk map area (104B/7E, 8W, 9W, 10E): British Columbia Ministry of Energy, Mines and Petroleum Resources, Geological Fieldwork 1988, Paper 1989-1, p. 241–250.

Britton, J.M., Blackwell, J.D., and Schroeter T.G., 1990, #21 zone deposits, Eskay Creek, northwestern British Columbia: British Columbia Ministry of Energy, Mines and Petroleum Resources, Exploration in British Columbia 1989, p. 197–223.

Bergman Weihed, J., Bergstöm, U., Billström, K., and Weihed, P., 1996, Geology, tectonic setting, and origin of the Paleoproterozoic Boliden Au-Cu-As deposit, Skellefte district, northern Sweden: Economic Geology, v. 91, p. 1073–1097.

Board, W.S., McLeish, D.F., Greig, C.J., Bath, O.E., Ashburner, J.E., Murphy, T., and Friedman, R.M., 2020, The Brucejack Au-Ag deposit, northwest British Columbia, Canada: multistage porphyry to epithermal alteration, mineralization, and deposit formation in an island-arc setting: SEG Special Publication, v. 23, p. 289–311.

Childe, F., 1996, U-Pb geochronology and Nd and Pb isotope characteristics of the Au-Ag-rich Eskay Creek volcanogenic massive sulfide deposit, British Columbia. Economic Geology, v. 91, p. 1209–1224.

Colpron, M., and Nelson, J.L., 2011, A digital atlas of terranes for the northern Cordillera: British Columbia Ministry of Energy and Mines, GeoFile 2011-11.

Dubé, B., Mercier-Langevin, P., Hannington, M., Lafrance, B., Gosselin, G., and Gosselin, P., 2007, The LaRonde Penna world-class Au-rich volcanogenic massive sulfide deposit, Abitibi, Québec: Mineralogy and geochemistry of alteration and implications for genesis and exploration: Economic Geology, v. 102, p. 633–666.

Franklin, J.M., Gibson, H.L., Jonasson, I.R., and Galley, A.G., 2005, Volcanogenic massive sulfide deposits: Economic Geology, 100th Anniversary Volume, p. 523–560.

Fuchs, S., Hannington, M.D., and Petersen, S., 2019, Divining gold in seafloor polymetallic massive sulfide systems: Mineralium Deposita, v. 54, p. 789–820.

Gagnon, J.F., and Waldron, J.W.F., 2011, Sedimentation styles and depositional processes in a Middle to Late Jurassic slope environment, Bowser Basin, northwestern British Columbia, Canada: Marine and Petroleum Geology, v. 28, p. 698–715.

Gagnon, J.F., Barresi, T., Waldron, J.W.F., Nelson, J.L., Poulton, T.P., and Cordey, F., 2012, Stratigraphy of the upper Hazelton Group and the Jurassic evolution of the Stikine terrane, British Columbia: Canadian Journal of Earth Sciences, v. 49, p. 1027–1052.

Gammons, C.H., and Barnes, H.L., 1989, The solubility of Ag_2S in near-neutral aqueous sulfide solutions at 25 to 300°C: Geochimica et Cosmochimica Acta, v. 53, p. 279–290.

Gibson, H.L., Kerr, D.J., and Cattalani, S., 2000, The Horne mine: Geology, history, influence on genetic models, and a comparison to the Kidd Creek Mine: Exploration and Mining Geology, v. 9, p. 91–111.

Govindarao, B., Pruseth, K.L., and Mishra, B., 2018, Sulfide partial melting and chalcopyrite disease: an experimental study: American Mineralogist, v. 103, p. 1200–1207.

Hannington, M.D., 2014, Volcanogenic massive sulfide deposits: Treatise on Geochemistry, v. 13, p. 463–488.

Hannington, M.D., Jonasson, I.R., Herzig, P.M., and Petersen, S., 1995, Physical and chemical processes of seafloor mineralization at mid-ocean ridges: Geophysical Monograph Series, v. 91, p. 115–157.

Healy, R.E., and Petruk, W., 1990, Petrology of Au-Ag-Hg alloy and "invisible" gold in the Trout Lake massive sulfide deposit, Flin Flon, Manitoba: Canadian Mineralogist, v. 28, p. 189–206.

Huston, D.L., 2000, Gold in volcanic-hosted massive sulfide deposits: Distribution, genesis, and exploration: Economic Geology Reviews, v. 13, p. 401–426.

Huston, D.L., Bottrill, R.S., Creelman, R.A., Zaw, K., Ramsden, T.R., Rand, S.W., Gemmell, J.B., Jablonski, W., Sie, S.H., and Large, R.R., 1992, Geologic and geochemical controls on the mineralogy and grain size of gold-bearing phases, eastern Australian volcanic-hosted massive sulfide deposits: Economic Geology, v. 87, p. 542–563.

Idziszek, C., Blackwell, J., Fenlon, R., McArthur, G., and Mallo, D., 1990, The Eskay Creek discovery: Mining Magazine, March 1990, p. 172–173.

Kerr, D.J., and Mason, R., 1990, A re-appraisal of the geology and ore deposits of the Horne mine complex at Rouyn-Noranda, Quebec: Canadian Institute of Mining Metallurgy Special Volume, v. 43, p. 153–165.

Krushnisky, A., Mercier-Langevin, P., Ross, P.S., Goutier, J., McNicoll, V., Moore, L., Monecke, T., Jackson, S.E., Yang, Z., Petts, D.C., and Pilote, C., 2023, Geology and controls on gold enrichment at the Horne 5 deposit and implications for the architecture of the gold-rich Horne volcanogenic massive sulfide complex, Abitibi Greenstone Belt, Canada: Economic Geology, v. 118, p. 285–318.

Kyba, J., and Nelson, J., 2015, Stratigraphic and tectonic framework of the Khyber-Sericite-Pins mineralized trend, lower Iskut River, northwest British Columbia: British Columbia Ministry of Energy and Mines, Geological Fieldwork 2014, Paper 2015-1, p. 41–58.

Large, R.R., Gemmell, J.B., and Paulick, H., 2001, The alteration box plot: a simple approach to understanding the relationship between alteration mineralogy and lithogeochemistry associated with volcanic-hosted massive sulfide deposits: Economic Geology, v. 96, p. 957–971.

Larocque, A.C.L., and Hodgson C.J., 1993, Gold distribution in the Mobrun volcanic-associated massive sulfide deposit, Noranda, Quebec: a preliminary evaluation of the role of metamorphic remobilization: Economic Geology, v. 88, p. 1443–1459.

Lindsay, D., Prowse, N.D., DeDecker, J., Mitchell, A.J., and Kim, R.S.Y., 2021, NI 43-101 Technical report on the SIB-Corey-North Mitchell property, Eskay Mining Corp., 204 p.

Longerich, H.P., Jackson, S.E., and Günther, D., 1996, Laser ablation inductively coupled plasma mass spectrometric transient signal acquisition and analyte concentration calculation: Journal of Analytical Atomic Spectrometry, v. 11, p. 899–904.

Loucks, R.R., and Mavrogenes, J.A., 1999, Gold solubility in supercritical hydrothermal brines measured in synthetic fluid inclusions: Science, v. 284, p. 2159–2163.

MacDonald, A.J., 1993, Lithostratigraphy and geochronometry, Brucejack Lake, northwestern British Columbia (104B/08E): British Columbia Ministry of Energy, Geological Fieldwork 1992, Paper 1993-1, p. 315–323.

MacDonald, A.J., Lewis, P.D., Thompson, J.F.H., Nadaraju, G., Bartsch, R.D., Bridge, D.J., Rhys, D.A., Roth, T., Kaip, A., Godwin, C.I., and Sinclair, A.J., 1996, Metallogeny of an

Early to Middle Jurassic arc, Iskut River area, northwestern British Columbia. Economic Geology, v. 91, p. 1098–1114.

Marsden, H., and Thorkelson, D.J., 1992, Geology of the Hazelton volcanic belt in British Columbia: Implication for the Early to Middle Jurassic evolution of Stikinia: Tectonics, v. 11, p. 1266–1287.

Marshall, B., and Gilligan, L.B., 1987, An introduction to remobilization: Information from ore-body geometry and experimental considerations: Ore Geology Reviews, v. 2, p. 87–131.

Marshall, B., and Gilligan, L.B., 1993, Remobilization, syn-tectonic processes and massive sulphide deposits: Ore Geology Reviews, v. 8, p. 39–64.

Marshall, B., Vokes, F.M., and Larocque, A.C.L., 2000, Regional metamorphic remobilization: upgrading and formation of ore deposits: Reviews in Economic Geology, v. 11, p. 19–38.

McLeish, D., Williams-Jones, A.E., Vasyukova, O.V., and Board, W.S., 2021, Colloidal transport and flocculation are the cause of the hyperenrichment of gold in nature: PNAS, v. 118, e2000689118.

McNicoll, V., Goutier, J., Dubé, B., Mercier-Langevin, P., Ross, P.S., Dion, C., Monecke, T., Legault, M., Percival, J., and Gibson, H., 2014, U-Pb geochronology of the Blake River group, Abitibi Greenstone Belt, Quebec, and implications for base metal exploration: Economic Geology, v. 109, p. 27–59.

Mercier-Langevin, P., Dubé, B., Hannington, M.D., Davis, D.W., Lafrance, B., and Gosselin, G, 2007, The LaRonde Penna Au-rich volcanogenic massive sulfide deposit, Abitibi Greenstone Belt, Quebec: Part 1. Geology and geochronology: Economic Geology, v. 102, p. 585–609.

Mercier-Langevin, P., Hannington, M.D., Dubé, B., and Bécu, V., 2011, The gold content of volcanogenic massive sulfide deposits: Mineralium Deposita, v. 46, p. 509–539.

Mercier-Langevin, P., McNicoll, V., Allen, R.L., Blight, J.H.S., and Dube, B., 2013, The Boliden gold-rich volcanogenic massive sulfide deposit, Skellefte district, Sweden: New U–Pb age constraints and implications at deposit and district scale: Mineralium Deposita, v. 48, p. 485–504.

Meuzelaar, T., 2015, Hydrothermal alteration of carbonaceous mudstones hosting the Eskay Creek Au deposit, British Columbia: PhD thesis, Golden, Colorado, The Colorado School of Mines, 195 p.

Monecke, T., Gale, D., Roth, T., and Hannington, M.D., 2005, The submarine volcanic succession hosting the massive sulfide and sulfosalt Eskay Creek deposit, Canada. In: Y. Mao, F.P., Bierlein (eds.) Mineral Deposit Research: Meeting the Global Challenge. Proceedings of the 8th biennial SGA meeting, Beijing, China (August 18–21, 2005). Springer, p. 655–658.

Monecke, T., Gibson, H., Dubé, B., Laurin, J., Hannington, M.D., and Martin, L., 2008, Geology and volcanic setting of the Horne deposit, Rouyn-Noranda, Quebec: Initial results of a new research project. Geological Survey of Canada Current Research 2008-9, 16 p.

Monecke, T., Petersen, S., and Hannington, M.D., 2014, Constraints on water depth of massive sulfide formation: evidence from modern seafloor hydrothermal systems: Economic Geology, v. 109, p. 2079–2101.

Monecke, T., Gibson, H.L., and Goutier, J., 2017, Volcanogenic massive sulfide deposits of the Noranda camp: Reviews in Economic Geology, v. 19, p. 169–223.

Mortensen, J.K., Gemmell, J.B., McNeill, A.W., and Friedman, R.M., 2015, High-precision U-Pb zircon chronostratigraphy of the Mount Read Volcanic Belt in Western Tasmania,

Australia: Implications for VHMS deposit formation: Economic Geology, v. 110, p. 445–468.

Nagase, T., and Kojima, S., 1997, An SEM examination of the chalcopyrite disease texture and its genetic implications: Mineralogical Magazine, v. 61, p. 89–97.

Nelson, J.L., and Kyba, J. 2014, Structural and stratigraphic control if porphyry and related mineralization in the Treaty Glacier-KSM-Brucejack-Stewart trend of northwestern Stikinia: British Columbia Ministry of Energy and Mines, Geological Fieldwork 2013, Paper 2014-1, p. 111–140.

Nelson, J.L., Colpron, M., and Israel, S., 2013, The cordillera of British Columbia, Yukon and Alaska: Tectonics and metallogeny: Society of Economic Geologists, Special Publication, v. 17, p. 53–103.

Nelson, J., Waldron, J., van Straaten, B., Zagorevski, A., and Rees, C., 2018, Revised stratigraphy of the Hazelton Group in the Iskut River region, northwestern British Columbia: British Columbia Geological Survey, Paper 2018-1, p. 15–38.

Norris, J.R., Tosdal, R.M., Lipske, J., and Wilson, A.J., 2023, Late-stage low-temperature hydrothermal alteration overprint at the east zone in the Red Chris porphyry Cu-Au deposit, northwestern British Columbia, Canada: Economic Geology, v. 118, p. 391–409.

Peterson, M., 2022, Geology, alteration, and sulfide mineralization of the TV and Jeff precious-metal occurrences in northwestern British Columbia, Canada: M.Sc. thesis, Golden, Colorado, The Colorado School of Mines: 96 p.

Prowse, N., Kim, R., DeDecker, J., and Mitchell, A., 2023, Assessment report describing 2021 diamond drilling, soil sampling, and geological mapping at the TV-Jeff, Corey, and AP Zone/Scarlet Ridge prospects on the SIB-Corey-North Mitchell property: Eskay Mining Corp., 138 p.

Rees, C., Riedell, K.B., Proffett, J.M., Macpherson, J., and Robertson, S., 2015, The Red Chris porphyry copper-gold deposit, northern British Columbia, Canada: Igneous phases, alteration, and controls of mineralization: Economic Geology, v. 110, p. 857–888.

Roth, T., Thompson, J.F.H., and Barrett, T.J., 1999, The precious metal-rich Eskay Creek deposit, northwestern British Columbia: Reviews in Economic Geology, v. 8, p. 357–373.

Schardt, C., Cooke, D.R., Gemmell, J.B., and Large, R.R., 2001, Geochemical modeling of the zoned footwall alteration pipe, Hellyer volcanic-hosted massive sulfide deposit, Western Tasmania, Australia: Economic Geology, v. 96. p. 1037–1054.

Sherlock, R.L., Roth, T., Spooner, E.T.C., and Bray, C.J., 1999, Origin of the Eskay Creek precious metal-rich volcanogenic massive sulfide deposit: fluid inclusion and stable isotope evidence: Economic Geology, v. 94, p. 803–824.

Taube, A., 1986, The Mount Morgan gold-copper mine and environment, Queensland: a volcanogenic massive sulfide deposit associated with penecontemporaneous faulting: Economic Geology, v. 81, p. 1322–1340.

Tipper, H.W., and Richards, T.A., 1976, Jurassic stratigraphy and history of north-central British Columbia: Geological Survey of Canada Bulletin, v. 270, 82 p.

Tombe, S.P., Richards, J.P., Greig, C.J., Board, W.S., Creaser, R.A., Muehlenbachs, K.A., Larson, P.B., DuFrane, S.A., and Spell, T., 2018, Origin of the high-grade early Jurassic Brucejack epithermal Au-Ag deposits, Sulphurets mining camp, northwestern British Columbia: Ore Geology Reviews, v. 95, p. 480–517.

Tomkins, A.G., 2007, Three mechanisms of ore re-mobilisation during amphibolite facies metamorphism at the Montauban Zn-Pb-Au-Ag deposit: Mineralium Deposita, v. 42, p. 627–637.

Vokes, F.M., and Craig, J.R., 1993, Post-recrystallization mobilisation phenomena in metamorphosed stratabound sulphide ores: Mineralogical Magazine, v. 57, p. 19–28.

Voudouris, P.C., Spry, P.G., Sakellaris, G.A., and Mavrogonatos, C., 2011, A cervelleite-like mineral and other Ag-Cu-Te-S minerals [Ag_2CuTeS and $(Ag,Cu)_2TeS$] in gold-bearing veins in metamorphic rocks of the Cycladic Blueschist Unit, Kallianou, Evia Island, Greece: Mineralogy and Petrology, v. 101, p. 169–183.

Wagner, T., Jonsson, E., and Boyce, A.J., 2005, Metamorphic ore remobilization in the Hällefors district, Bergslagen, Sweden: constraints from mineralogical and small-scale sulphur isotope studies: Mineralium Deposita, v. 40, p. 100–114.

Wagner, T., Klemd, R., Wenzel, T., and Mattsson, B., 2007, Gold upgrading in metamorphosed massive sulfide ore deposits: Direct evidence from laser-ablation-inductively coupled plasma-mass spectrometry analysis of invisible gold: Geology, v. 25, p. 775–778.

Wilkin, R.T., and Barnes, H.L., 1997, Formation processes of framboidal pyrite: Geochimica et Cosmochimica Acta, v. 61, p. 323–339.

Wilson, S.A., Ridley, W.I., and Koenig, A.E., 2002, Development of sulfide calibration standards for the laser ablation inductively-coupled plasma mass spectrometry technique: Journal of Analytical Atomic Spectrometry, v. 17, p. 406–409.

APPENDIX A

SUPPLEMENTAL FILES

File name	**Description**
Sample_list_TV_Jeff.xls	List of samples and thin sections
EMPA_TV_Jeff.xls	Microprobe analyses of ore minerals
LAICPMS_TV_Jeff.xls	LA-ICP-MS analyses of pyrite
Copyright_Permission	Peterson (2022) copyright permission